Santa Catalina Mountains – Jemez River Basin CZO

Annual Report, June 15, 2014

Major Goals of SCM-JRB CZO

The proposed work aims to improve our understanding of the mechanisms underlying quantitative relations between climatic forcing and critical zone evolution by focusing on linkages between long time-scale climate/lithology interactions and short time-scale ecological/geological feedbacks, and how both affect CZ services. This goal motivates the proposal's central thematic questions:

1) How do the long-term drivers of CZ structure and function (EEMT and tectonics) alter parent material to control current CZ structure and response to perturbation?

2) How is long-term CZ evolution affected by ecosystem process controls, including especially localized plant and microbial activities?

3) What is the impact of CZ structure on buffering climate- and disturbance-driven variability in water, soil and vegetation resources and how does this translate into changes in CZ services?

Specific Objectives

The specific objectives of the current CZO grant can be concisely articulated as follows (for details, see proposal):

1. Conduct geophysical characterization of the subsurface.
2. Conduct drill core extractions and borehole instrumentations
3. Conduct extracted core characterizations.
4. Observe water and carbon pulse to the deep CZ.
5. Determine decadal- and millennial-scale erosion rates.
6. Quantify lithologic controls on CZ structure and function.
7. Measure disturbance-induced change in topography via fire.
8. Assess fire-induced flux changes and post-fire vegetation recovery.
9. Conduct a dendrochonological fire disturbance history.
10. Measure dust inputs and dynamics.
11. Conduct pedon-scale EEMT estimation.
12. Measure time-resolved biogeochemical dynamics in convergent zones.
13. Assess microbial distribution and role in CZ response.

14. Complete distributed measurements of component water and CO2 fluxes.
15. Quantify variability in water cycle.
16. Quantify carbon and water fluxes.
17. Measure soil C storage.
18. Obtain improved time resolution of stream water response.
19. Continue improvements to EEMT modeling.
20. Execute numerical model of the coevolution of topography and soils.
21. Test for controls on mean water transit times.
22. Build a terrestrial integrated modeling system (TIMS) by coupling existing process-based models across disciplines and testing against various CZ measurements .
23. Incorporate snow-vegetation-carbon-water interactions via SNOWPALM model.
24. Model fluid flow convergence for likely hot spots.
25. Measure concentration-discharge relations for the subsurface.
26. Assess fire impacts downstream.

SCM-JRB Major Activities

•Upgraded sap flux measurements associated with Bigelow Tower.

•Monitored plant physiological performance across seasonal periods. We used leaf-level gas exchange measurements on 24 trees across a range of temperatures to quantify this plant temperature sensitivity during the dry pre-monsoon and wet monsoon seasons.

•Measured transpirational water loss and photosynthetic carbon uptake across seasonal periods of variable precipitation to examine interspecific differences in rates of water loss and carbon uptake efficiency.

•Used the Bigelow Flux tower as a location for lab courses to meet for (1) GEOG 438/538 Biogeography, (2) ECOL 463/563 Ecology and Natural History of the Sonoran Desert and Upper Gulf of California, and (3) the Mount Lemmon Sky Center, which provides day-long and overnight hands on science excursions for middle schoolers.

•Preparation and preliminary installation of microclimate array at the Zero Order Basin (ZOB) sites in SCM (**Figure 1**). Current activities on microclimate array installation include: (i) Hemispherical photography at multiple locations within ZOB for site selection; (ii) Acquisition of all instrumentation for microclimate array installation; (iii) Installation of wind profile set-up on site (to estimate wind profile attributes: roughness length,

friction velocity) to determine proper sensor instrumentation height; (iv) Data logger programming for sensor installation; (v) Lab trials for sensor functioning and calibration.

- Evaluated sediment deposition onto litter for simulated and natural rain and wind events for three Sonoran Desert litter types (grass, shrub leaves, shrub twigs) and three dryland soils.

- Conducted a cross-site comparison of particulate organic matter flux in streamflow in disturbed and undisturbed catchments (including SCJ CZO, BCCZO and WY sites), initiated by an undergraduate honor student.

- Intensive surveying and analyses were completed to quantify particulate organic matter transport and deposition in debris flows following fire (SCJ CZO).

- A cross site comparative project quantifying carbon storage in biomass (SCJ and BC CZO sites) was initiated.

- A project describing the seasonal, climatic, and topographical controls on streamwater carbon export in the Jemez sites was completed.

- A cross site comparison of snowmelt timing and soil moisture in western CZO sites (SCJ, SS, BC CZO sites) was completed.

- A comparison of snowpack sublimation and melt rates in the intermountain west was completed.

- Initiated an effort to secure Airborne Electromagnetic (AEM) surveys for CZO sites together with Steve Holbrook (University of Wyoming, USA) and Esben Auken (Aarhus University, Denmark).

- The effect of landscape position and EEMT, on water residence time and mineral weathering fluxes around Redondo Peak (catchment-scale) and at the pedon scale were quantified.

- Aspect controls on hydrologic partitioning and vegetation response were investigated at the catchment (three first order high elevation catchments around Redondo Peak) and East Fork Jemez River Basin scale.

- A study of the effect of wildfire on the chemistry and volume of precipitation, specifically throughfall and stemflow (sample set up and collector installation in prep) was initiated.

- Soil development and inputs of dust and volcanic ash was investigated in the MCZOB (pre-burn) using uranium-series isotopes.

- A Ph.D. thesis project was initiated to test the hypothesis that headwater springs are important contributors to the East Fork-Jemez river (EFJR) that flows through the Valles Caldera National Preserve, and hence EFJR water chemistry variability can be explained by chemical composition of those headwaters (**Figure 2**).

- Microbial enzyme models were developed for simulating soil microbial respiration pulses (a.k.a. the "Birch effect") and models assessed against field measurements.

- Developing a radiation correction scheme that accounts for the effects of slope angle/aspects and shading and further implementing the scheme into our Terrestrial Integrated Modeling System (TIMS) to study the effects of complex terrain on snow accumulation and ablation as well as snowmelt runoff.

- Trained undergraduate students in collection and management of meteorological data sets and data from time-lapse digital images.

- Quantified the magnitude of post-wildfire erosion in selected areas of the Jemez Mtns. following the Thompson Ridge wildfire using terrestrial laser scanning. Data will constrain a new model of how post-wildfire erosion rates vary with terrain slope and burn severity in upland hillslopes

- Completed a post-wildfire change-detection analysis of 197 km2 burned by the Las Conchas fire using multi-temporal airborne laser scanning (ALS) data

- Completed a post-wildfire change-detection analysis of the response of two piedmonts (fans) that experienced large pulses of sediment following the Las Conchas fire using multi-temporal terrestrial laser scanning (TLS) data

- Completed a study of the dependence of erosion rate on time scale in the Jemez Mtns. over 6 orders of magnitude of time scales (100 -106 yr).

- Completed a study that develops the use of NEXRAD data to quantify the scaling of flood magnitudes across 5 orders of magnitude of drainage basin area

- Completed a seismic refraction analysis of regolith thickness on hillslopes and valley bottoms of varying terrain slope and aspect in three watersheds of the Jemez Mtns.

- Led an international workshop on the prediction of geomorphic response to changing climates and land use

- Led an international CZO workshop on "Drilling the Ridge" prior to the GSA meeting in Denver, October 2013.

- Pelletier and Swetnam co-led CZO lidar workshop with Adrian Harpold in May, 2014. This provided training and development for all levels of CZO researchers.

- Developed a one-day "stream table" lesson for grades 1-5 illustrating interactions of precipitation, erosion, slope, and vegetation. Implemented this lesson (leading one lesson and training teachers in the implementation of this lesson) at Tanque Verde Elementary School.

- Used digital soil mapping techniques to predict soil physical, chemical, and biological properties as continuous variables across a forested, granitic catchment in Marshall Gulch in the Santa Catalina Mountains (SCM).

- Quantified mineral weathering in bulk soil profiles and at the grain scale across the entire climate gradient encompassed by the SCM for convergent and divergent landscape positions.

- Quantified soil C physical distribution and residence time for convergent and divergent landscape positions across the entire SCM climate gradient.

- Modeled the effect of topography, vegetation, and disturbance on the rate of effective energy and mass transfer (EEMT) to the critical zone for the Sabino Creek Watershed in the SCM.

- Conducted field survey of infiltration rates after high-intensity burn (in 2013). This survey was conducted at locations (±1m) where earlier surface infiltration measurements were conducted

- Calibration and data quality assessment of the VC soil moisture sensors.

- Modeling of subsurface vadose zone hydrological dynamics, using moisture sensors, observed precipitation and transpiration rates and pedological information.

- Developed a remote sensing algorithm for individual tree detection in the SCM-JRB CZO sites.

- Reported on the scaling behavior of forest structure in the SCM-JRB CZO.

- Developed an extension to the Metabolic Scaling Theory which incorporates the effects of exogenous disturbance on forest structure.

- Developed a method for discriminating variation in forest structure using local indicators of spatial association, i.e. Getis-Ord Gi* and Anselin's Moran I, which can be used to develop common stand exam polygons and identify previously unknown disturbance legacies in semi-arid forests.

•Quantified the total biomass across the SCM-JRB CZO using aerial LiDAR calibrated to plot based observations.

•Surveyed microbial community enzymatic activity across a post-fire burn gradient in the JRB MC-ZOB.

SCM-JRB CZO Results

• **Vegetation structure derived from LiDAR data:** Forest trees in water-limited ecosystems are simple to delineate using aerial LiDAR due to their generally open canopy cover percentage (**Fig. 3**). Forest size frequency distributions follow a predictable set of scaling rules that can be modeled with scale invariant distributions, i.e. tapered or truncated Pareto distributions (**Fig. 4**). Regardless of past disturbance history forests are shown to exhibit MST expected scaling (**Fig. 5**). Aboveground carbon storage in biomass is strongly related to landscape position with peak biomass storage located in toe slopes. Preliminary analyses or tree ring isotopes suggests that these areas are subject groundwater subsidy and vegetation is not water limited.

• **Ecohydrologic studies show strong effects of interannual climatic variation:** Multi-year comparisons of sap flux **(Fig. 6)** in the SCM Bigelow site show that winter 2013 was wetter and colder than 2014. Sap flux was suppressed until March, but then rose gradually into spring. In contrast, 2014 was dry and warm, yielding substantial sap flux throughout the winter, and by mid-May, rates approached zero as trees exhausted their water. Maximum photosynthetic rates were 51% higher during the monsoon than pre-monsoon, illustrating the influence of summer precipitation on photosynthetic potential. Additionally, the range of temperatures across which the overstory trees were able to assimilate carbon (Ω50) was 21% higher following the onset of monsoon rains with strong lithologic effects (**Fig. 7**). Transpirational water loss increased significantly due to the onset of the summer monsoon rainy season, as expected, but there were dramatic differences in the responsiveness of species to this renewed water resource (**Fig. 8**). These species-specific findings are particularly important because Forest Service management practices, such as reduced thinning and fire suppression, is yielding a community enriched in P. menziessii, as opposed to Pinus species.

• **Effects of fire on understory regrowth dynamics:** Understory growth dynamics in JRB mixed conifer forest following high severity burn (Las Conchas 2011 wildfire) are related to aspect and other environmental parameters. Ten phenocams at varying elevations and aspects took hourly images for a year post-fire (**Table 1**, also see YOUTUBE VIDEO: http://youtu.be/iTe5oj8rqHA). These images enabled observation of vegetation at any time of the year. A “greenness index” was calculated based on pixel RGB values. For all sites, soil moisture increases following spring snowmelt whereas only in the lower sites does soil moisture increase during monsoon season.

Greenness values of lower sites peak earlier in the year than for higher sites. West facing - but not east-facing - vegetation dynamics correlated with soil temperature. Vegetation regrowth is more successful in convergent flow locations, especially lower in the watershed. West-facing aspect recovery appears to be more successful than east-facing (**Figs. 9-10**). Allometric relationships are being established on a species-specific basis (**Fig. 11**) to predict sapwood cross-sectional area and better resolve sapflux and transpirational dynamics.

• **Central importance of snowpack to upland hydrology:** Snowmelt timing throughout the western CZO's is the primary control on soil moisture at all sites. Peak soil moisture occurs within days of the end of snowmelt with only small responses to summer rainfall. Sublimation amounts are increasing through much of the intermountain west, presumably in response to warming atmosphere and increasing vapor pressure deficits. Melt is not beginning earlier, but melt rates are faster resulting in a shorter snow covered season.

• **Interannual variation in hydrologic partitioning:** Three headwater catchments around Redondo Peak (JRB, La Jara, History Grove, Upper Jaramillo) investigated for hydrologic partitioning and vegetation response due to aspect had similar amounts of annual precipitation (**Fig. 12**) but showed significant interannual variability. Streamflow is dominated by baseflow year-round (8-14% of total precipitation), with Upper Jaramillo having the largest and least variable discharge over 5 years of study (2008-2012). Water vaporization (V in **Fig. 12**) from soil evaporation, interception, transpiration and sublimation, was smaller in the N-facing Upper Jaramillo catchment relative to the two south-facing catchments, La Jara and History Grove, consistent with lower solar radiation. The amount of water available for vegetation (W; catchment wetting) was above 98% of total precipitation in all 3 catchments. The Horton Index (V/W) was largest in the south-facing catchments (La Jara and History Grove), suggesting that vegetation use water more efficiently in the drier south facing catchment.

• **Aspect-induced variation in vegetation response:** Despite the variability in precipitation between 2008 and 2012, the average and standard deviation of NDVI did not change considerably in the 3 high elevation catchments nor the larger Jemez River Basin (**Fig. 13**). However, there were significant differences in NDVI between catchments (**Table 2**). The south facing catchments (La Jara and History Grove) show a larger vegetation response during the 12 years of analysis (2000-2012) consisting with the larger W term in the hydrological partitioning analysis. The north facing catchment (Upper Jaramillo) has a shorter duration of growing season than the south east facing catchments (**Table 2**). Precipitation and maximum NDVI are correlated for the entire East Fork Jemez Basin based on 12 years of data (**Fig. 14**). NDVI and Horton Index are also correlated (**Fig. 14**); NDVI decreases with dryness consistent with water-limited primary production, and vegetation uses water more efficiently with increasing dryness.

The full 32 year data record indicates a decreasing trend in average precipitation and an increasing trend in Horton index as the catchment becomes drier (**Fig. 15**).

• **Catchment-scale carbon balance indicates large pre-burn accretion rate:** Conjunctive use of (i) eddy covariance, (ii) LiDAR, (iii) soils and (iv) hydrologic datasets from the CZO indicate that the same three upland catchments in the JRB (LJ, HG, and UJ) operated (at least prior to Thompson Ridge wildfire of 2013) as massive carbon sinks with CZ carbon inputs >> outputs (**Fig. 16**). Particulate organic carbon and nitrogen fluxes peak during snowmelt, but are much lower than fluxes in lower elevation sites where peak fluxes occur in response to monsoon rainfall. C:N ratios suggest that the flush in high elevations systems is microbial in origin, where particulate C and N in low elevation sites are largely terrestrial. Inter-annual and intersite differences in streamwater carbon export, and thus sensitivity of carbon export to climate change, can be evaluated by simultaneously considering the role of water as 1) transporter, 2) reservoir, and 3) incubator of biogeochemical reactions (Perdrial et al., 2013).

• **Subsurface accumulations of carbon and weathering products depend on landscape position:** A novel digital soil mapping approach that includes an iterative data reduction routine was employed to predict the distribution in soil characteristics. Environmental/geospatial data were generated accounting for landscape variation using a conditioned Latin Hypercube sampling design, field sampling, and regression analyses. Spatial interpolation of regression residuals were used to predict a range of soil physical, chemical, and biological properties in a forested, granitic catchment in the SCM (**Fig. 17**).

• **Modeling of dry-pore accumulation of bioavailable organic matter improves simulations of respiration:** By assessing five evolving microbial enzyme models (or five hypotheses) over a wide range of model parameters, we found that models that include an additional carbon pool to accumulate degraded carbon in the dry zone of the soil pore space have a greater probability to reproduce the observed respiration pulses (**Fig. 18**). The degraded carbon accumulated in the dry zone during dry periods becomes immediately accessible to microbes in response to rainstorms, providing a major mechanism to generate respiration pulses. In addition, transition of degraded carbon and enzyme between the dry and wet soil zones and a linear soil moisture control on the rates of carbon decomposition and microbial uptake help improve the models' capability of simulating the "Birch effect" (**Fig. 18**).

• **Tritium age dating of JRB spring waters is consistent with higher water transit times on north facing slopes and greater water-rock contact time for weathering reactions:** Springs with north-facing contributing areas receive higher EEMT than south-facing springs (**Fig. 19**). This difference in EEMT appears to control spring water residence times as determined using water stable isotopes (Broxton et al., 2009) and tritium (**Fig. 20**). Groundwater flowing through

north-facing slopes is resident in the subsurface ca. 4 times longer than that in south-facing slopes. These longer transit times enhance silicate mineral weathering and lead to greater solute fluxes to streamflow (**Fig. 21**).

• **Pedon-scale EEMT affects local soil-water flux:** The predominant terrain aspect (based on a 10-m DEM from soil pits in the MC ZOB) controls EEMT, which then influences water flux, soil and vegetation response at the pedon-scale. Total snow sublimation determined by the SnowPALM model between Oct 2010 and Sep 2012 also correlates with EEMT. There is a difference of 50 mm in sublimation between the south facing pedon and the two east facing pedons. Total water fluxes between March 2011 and Sept 2012 measured with the passive capillary samplers (PCaps) were smaller in the east-facing (3 and 4) and larger in the west-facing (1 and 6) slope. The depth to the B1 layer is thicker and leaf area index is also larger in the south east facing soil pits (**Fig. 23**).

• **Modeling of EEMT spatial distribution now accounts for both topography and current vegetation structure:** We developed an approach to modeling EEMT at relatively high spatial resolution that accounts for variation in topographic controls and radiation, temperature, and water redistribution, and current vegetation structure. Ideal model output was compared with estimates of EEMT based on current vegetation structure, both for disturbed and undisturbed areas. Results indicate that the improved calculation effectively captures topographic variation and provides a measure of a potential EEMT rate to compare with current rates of EEMT that are based on current vegetative cover (**Fig. 24**).

• **Mineral weathering exhibits strong water limitation:** A combination of microprobe, elemental chemistry, and quantitative mineralogy was used to quantify the variation in mineral weathering across different landscape positions and climates in the SCM. The degree of mineral weathering, including chemical depletion and mineral transformation increased with greater water availability across the elevation gradient, and with greater water availability in convergent landscape positions in a given climate regime. The largest effect of landscape position was observed in the wettest, high elevation ecosystem (**Fig. 25**).

• **Convergent landscape positions are hotspots of carbon accumulation and stabilization:** The distribution of organic C in density and aggregate fractions (free light, occluded, and mineral associated) was determined for convergent and divergent landscape positions across the SCM climate gradient. In the conifer systems we found that convergent landscape positions were enriched in occluded and mineral carbon and that occluded carbon typically has the longest mean residence time (**Table 4**). The occluded fraction was largely charred material produced during wildfire. The combined data suggest that in conifer systems in the SCM, convergent landscape positions are hot spots of C accumulation and sequestration of charred materials.

• **Litter-soil physical mixing during precipitation events may lead to organic matter stabilization and could explain "apparent" litter loss attributed to photo-degradation:** We evaluated sediment deposition onto litter for simulated and natural rain and wind events for three Sonoran Desert litter types (grass, shrub leaves, shrub twigs) and three dryland soils. Litter type along with event type and duration (2 vs. 20 min), were associated with principal component analysis axis 1 (explaining 33% of variance in sediment deposition for simulated events); soil type was associated with axis 2 (25% of variance). Sediment deposition onto litter from simulated events was greater for 20 than 2 min duration for rain but not wind events, and did not vary consistently among soils. For a given event duration there was more total deposition for rain than wind (2 min: 0.79 g /10.8 dm2 39 plot for rain, 0.13 g for wind; 20 min: 1.69 g for rain, 0.18 g for wind). Sediment deposition from natural events was typically greater for rain than wind events. Longer simulated rain events yielded more deposition per event. Shorter but frequent wind events contributed most to extrapolated annual deposition.

• **Particulate organic matter fluxes transported in debris flows following forest fires were several orders of magnitude higher than background fluxes:** This is despite the fact that particulate C fluxes are small in comparison to the amount of carbon lost to combustion during the fire. However, organic matter deposition to debris fans and riparian areas in post fire flows is nitrogen-rich representing 60 to 400 kg N/ ha, or more than 100 years equivalent of atmospheric N deposition. These particulate N fluxes are likely responsible for the elevated streamwater N concentrations observed by our NM EPSCoR colleagues for months after the fire.

• **Fire did not significantly alter soil infiltration rates:** Even though overland flow intensity appears to increase, infiltration rates of the mineral soil were not significantly changed following the high-intensity Thompson Ridge (2013) wildfire that occurred in the JRB MC ZOB (**Fig. 26**). The removal via combustion of the organic forest floor and its water storage capability appears to be the reason why overland flow occurs. Modeling of subsurface hydrodynamics is difficult due to temporal variation of subsurface hydraulic properties, due to either cracking of the soil during the pre-monsoon period, or development of subsurface channels due to burrowing animals. This "finding" is supported by the infiltration measurements that show unusually high infiltration rates (**Fig. 26**) for the loamy soil found in most of the MC-ZOB area.

• **Combustion of the biomantle induces massive solute release into surface soils:** Large surficial increases in lithogenic and bioactive solute concentrations were observed immediately following fire in the MC ZOB (**Fig. 27**). Sample collections from 23 sites throughout the MC ZOB indicated localized hotspots in association with zones of greatest pre-burn biomass accumulation (**Fig. 28**).

• **Enzymatic activity of soil microbial community exhibits depth dependence:** Eighteen days after containment of the June 2013 Thompson Ridge Fire in the JRB MC-ZOB, we measured potential activities of seven hydrolytic enzymes from six different depth increments (0-2, 2-5, 5-10, 10-20, 20-30, 30-40 cm), collected across a gradient of burn severities, using established fluorometric techniques. Potential enzyme activity decreases with depth at approximate mean summer soil temperature (15°C) for enzymes β-Glucosidase (BG), β-D-Cellobiohydrolase (CB), and Leucine aminopeptidase (LAP) (**Fig. 29, Table 4**). BG, CB and LAP enzymes are involved in the degradation of sugar, cellulose and proteins respectively, and their activities are used to gain insight into microbial degradation controls over C and N substrates.

• **Potential enzyme activity is higher in convergent sites relative to planar sites:** Differences in enzyme activity varied with landscape position, specifically convergent versus planar landscape forms. Convergent sites had higher potential enzyme activity for all enzymes assayed with the exception of LAP, which was not statistically different **(Fig. 30, Table 4**). These preliminary results indicate that landscape position is likely to have a strong effect on biologically mediated decomposition processes, possibly a result of increased microbial biomass within convergent sites.

• **Stoichiometry of potential enzyme activities shows variance in resource acquisition potential with depth:** Enzyme acquisition ratios, i.e. the ratio of activities of enzymes involved in hydrolyzing C, N, or P, provides insight into metabolism of soil microbial communities for energy and nutrient acquisition. Shifts in enzyme stoichiometry have been used as indicators for nutrient limitation, with higher acquisition potential often interpreted as greater resources being allocated towards nutrient acquisition. Results show a potential shift in enzymatic acquisition of N relative to C with depth, suggesting that C is potentially more limiting at greater depth (**Fig. 31**). However, both C and N acquisition at depth appear less important than P acquisition (**Fig. 31**). There was no significant correlation between soil C:N ratio and enzyme C:N ratio ($p=0.8007$, **Fig. 32**). Conversely, relationships between soil C:P and enzyme C:P generated a significant negative correlation (R^2=-0.4123, $p<0.001$, **Fig. 32**) and relationships between soil N:P and enzyme N:P generated a significant positive correlation (R^2=2.2774e-13, $p<0.001$, **Fig. 32**).

• **Post-wildfire erosion is predominant over geological time scales:** Measurements of short-term erosion rates can only be reconciled with measurements of long-term rates if post-fire erosion at ca. centennial return frequencies are considered (**Fig. 34**).

• **Time scale of recovery and the functional form of the decrease in erosion rate following the Las Conchas wildfire in two drainage basins was quantified**: Erosion rate declines approximately exponentially with time with a recovery time of 1 yr (**Figs. 35-36**).

• **Documented the power-law scaling of precipitation intensity and the deviation of flood discharges from power-law scaling as a function of drainage basin area for different recurrence intervals out to 500 yr (using a new analysis technique for NEXRAD data).**

• **Developed an empirical model for the relationships among post-fire erosion rate, terrain slope, and burn severity at the hillslope scale using TLS data following the Thompson Ridge fire:** Developed an empirical model that can be used for post-wildfire flood hazard assessment that quantifies post-wildfire erosion as a power-law function of average terrain slope and burn severity within watersheds (**Figs. 37-38**).

• **Developed a conceptual framework for Critical Zone Services and their relationship to Ecosystem Services:** This framework seeks to 1) expand the scope of ecosystem services by specifying how critical zone processes extend context both spatially and temporally, 2) determine constraints that limit rates of key processes, and 3) offer a potentially powerful currency for needed valuation (**Fig. 39**).

Training Activities

• CZO faculty, postdocs and graduate students mentored six undergraduate students from five different undergraduate institutions as part of the Biosphere 2 REU/RET program (All).

• Project provided UA postdoc, Jason Field, with training and experience in preparation of peer-reviewed manuscript for the Vadose Zone Journal, which is currently being revised for resubmission as a Priority Communication. Provided UA postdoc Tyson Swetnam with opportunities to analyze LiDAR data for publications related to biomass and carbon cycle assessments.

• Project provided laboratory and field based research experiences for 10 undergraduate students in activities ranging from field soil, water and biomass sample collection to their wet chemical, spectroscopic and isotopic analysis in UA laboratories.

•Undergraduate students developed independent research projects and presented these at various symposia.

• Project provided laboratory and field based research experience for 8 graduate students who conducted field sampling, datalogger downloading, and laboratory-based analyses as part of the CZO project.

• Becky Hall, a recent graduate from the University of Arizona, who is interested in pursuing graduate studies, has been incorporated in the team, gaining skills on microclimatic data acquisition and process, hemispherical photography, field installation, data logger programming.

• A new collaboration with the Salt River Project focused on the hydrological effects of forest thinning and forest management on water resources in the 4FRI forest management area of Northern Arizona (Paul Brooks).

• Five students were trained in the use of TLS in a research-based course and as part of an REU program at Biosphere 2 (Pelletier).

• Pelletier and Swetnam acted as instructors in CZO lidar workshop led by Adrian Harpold in May, 2014. This provided training and development for all levels of CZO researchers.

• Rebecca Lybrand received travel funding to attend the Soil Carbon Sequestration International Conference (2013) and SoilTrEC's workshop on Land-use and the sustainable use of soils in Iceland.

Outreach:

• Developed a one-day "stream table" lesson for grades 1-5 illustrating interactions of precipitation, erosion, slope, and vegetation. Implemented this lesson (leading one lesson and training teachers in the implementation of this lesson) at Tanque Verde Elementary School (Pelletier).

• Presented to 25 Biosphere 2 tour guides on "the important role of microbes in the Earth system" (Niu).

• University of Arizona Sky School Fellow: Rebecca Lybrand was recruited as a science outreach graduate fellow for a program focused on connecting K-12 students to outdoor science through 1-5 day science education programs at the Mt. Lemmon Sky Center in southern Arizona (near the SCM CZO). Oversaw multi-day soils research projects (4-5 students per group) where students brainstormed research questions, developed hypotheses, designed a short field study, conducted field work, synthesized results, and presented findings in a talk given to classmates and teachers.

• University of Arizona CLIMAS (Climate Assessment for the Southwest) Fellow Lybrand received fellowship funding to produce two short soils films that document the field work of a soil scientist using an energetic, first-person perspective. The film is focused on sites spanning the Santa Catalina Critical Zone Observatory. The objective of the work is to collaborate with UA Communications faculty to design "science message" and "science story" film scripts to evaluate the effectiveness of contrasting narrative strategies when teaching science. Surveys of elementary to undergraduate students will be conducted to understand which narrative strategies are most useful for communicating soils research and climate science. The products of this work will be digital films that are to be readily distributed using social media and other electronic methods of distribution (i.e., departmental websites).

• University of Arizona/NASA Space Grant Graduate Fellow: Through this project, Rebecca Lybrand designed and received funding to implement an educational outreach program focused on promoting the understanding of space science and space-related fields to underrepresented youth. Developed "Space to Soil" science activities and planned an associated field trip for the StrengthBuilding Partners i-STEM mentoring program (~60 Hispanic/Native American mentees and ~60 community and tribal mentors). Worked with a team of University of Arizona education specialists and Native American tribal members to ensure "Space to Soil" mentee science activities were accessible and relevant to underrepresented youth in the local community.

• Outreach leads Shipherd Reed and Bill Plant worked with researchers to gather important CZO ideas that we want to communicate through CZO Outreach and Education, refined to three key ideas, reviewed approach with researchers.

• Bill Plant revised concept and design for new exhibit “Welcome to the Critical Zone”

• Exhibit shifted from single person, digital experience to multi-person low tech experience to convey an immersive feel and offer opportunities to highlight the cross-disciplinary nature of Critical Zone science. Still included will be the “Critical Zone Survival” computer interactive game, in addition to immersive mural backdrop “Maze” and interpretive graphics, audio and video.

• Met with experienced informal science educators from successful Mt. Lemmon SkySchool program to develop activity ideas for the “Crititcal Zone Discovery” Program. Identified curriculum development personnel.

• Developing Mt. Lemmon Science Tour mobile app that will highlight Critical Zone science, including Soil section, including key graphics and motion graphics

• Developing mobile Critical Zone Science podcast as in-depth “follow up” to the Mt. Lemmon Science Tour app.

• Accompanied researchers and field technicians to record media from field research sites.

• Critical Zone researcher Paul Brooks presented in “water” themed Science Café series, video of his presentation on the importance of snow to water supply will be distributed through Flandrau Science Center YouTube channel.

• Extensive new coverage of the CZO project and what is was revealing about the role of fire in surface earth systems was included in the Arizona Daily Star and Arizona Republic newspapers following the 2013 Thompson Ridge wildfire in the JRB CZO.

Selected plans for the next year (Oct 1, 2014-Sept 30, 2015)

1. Installation of a mixed conifer control (unburned) site in the JRB: Since a major wildfire burned through our previously 'unburned' site containing eddy covariance tower, sapflux array, meteorological stations, subsurface moisture, potential and pore water sensors and samplers, we are in need of a new unburned site for direct comparison. This installation was previously unforeseen.
2. Completion of the Bigelow ZOB (SCM) installations, including all soil gas samplers and soil solution samplers.
3. Installation of redox electrodes in postulated 'hot spots' to accompany other instrumentation.
4. Installation of microclimate array at the Bigelow ZOB (SCM) site.
5. Complete a snow survey in the JRB to examine the current status of wildfire effects and to continue the data acquisition on inter-annual variation of snow water equivalent inputs.
6. Construct digital regolith maps showing property spatial distributions across the CZO and in collaboration with other CZOs.
7. Lead a cross-CZO effort on analysis of concentration discharge relations across the network.
8. Collaborate with WyCEHG on geophysical analyses as a function of aspect on Redondo massif to continue to assess postulated relations between aspect variation and regolith depth / water transit time.
9. Develop location and plans for deep drilling, borehole sample collection, and borehole instrumentation.
10. Measure the post-fire recovery of microbial community activity (as determined through enzyme assays and molecular ecology methods) in the JRB MC ZOB and provide direct comparisons to unburned controls.
11. Assess the impacts of fire on throughfall and stemflow chemistry.
12. Quantify the impacts of upland springs and streams on East Fork Jemez River water quality through an end-member mixing analysis.
13. Test the coupled NoahMP/Cathy model against data streams in Marshall Gulch (SCM) and La Jara (JRB) catchments, including resolving the carbon pool requirements needed for accurate modeling of soil respiration and CO_2 release.
15. Install the CZO gamma counter and initiate ^{137}Cs measurements on soil and sediment samples to quantify erosion rates.
16. Write manuscripts and submit papers for publication from prior CZO research.
17. Complete the Mount Lemmon iPhone APP for the Santa Catalina Mountains.
18. Pursue installation of the CZ science exhibit in the Flandrau Science Museum.

Figures file to accompany Santa Catalina – Jemez CZO Annual Report
June 15, 2014

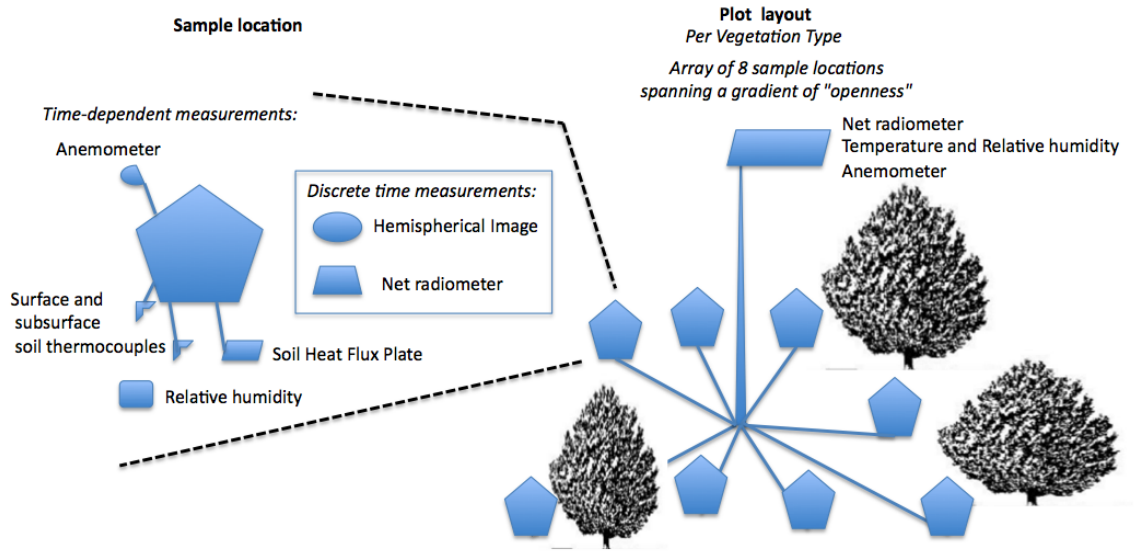

Figure 1. Microclimate array components (Breshears et al).

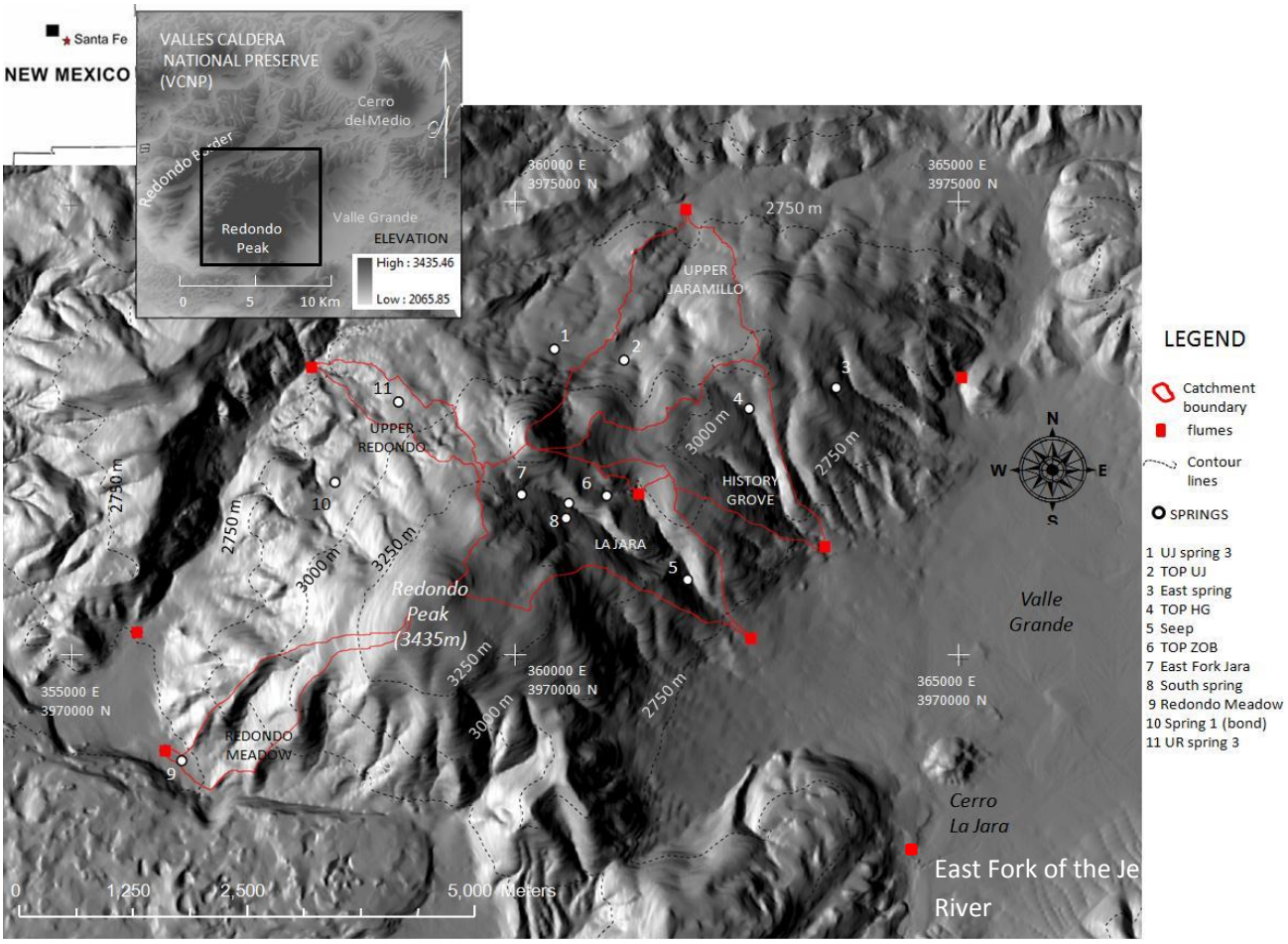

Figure 2. Spring and flume locations being sampled to explain EFJR chemistry (Meixner et al.).

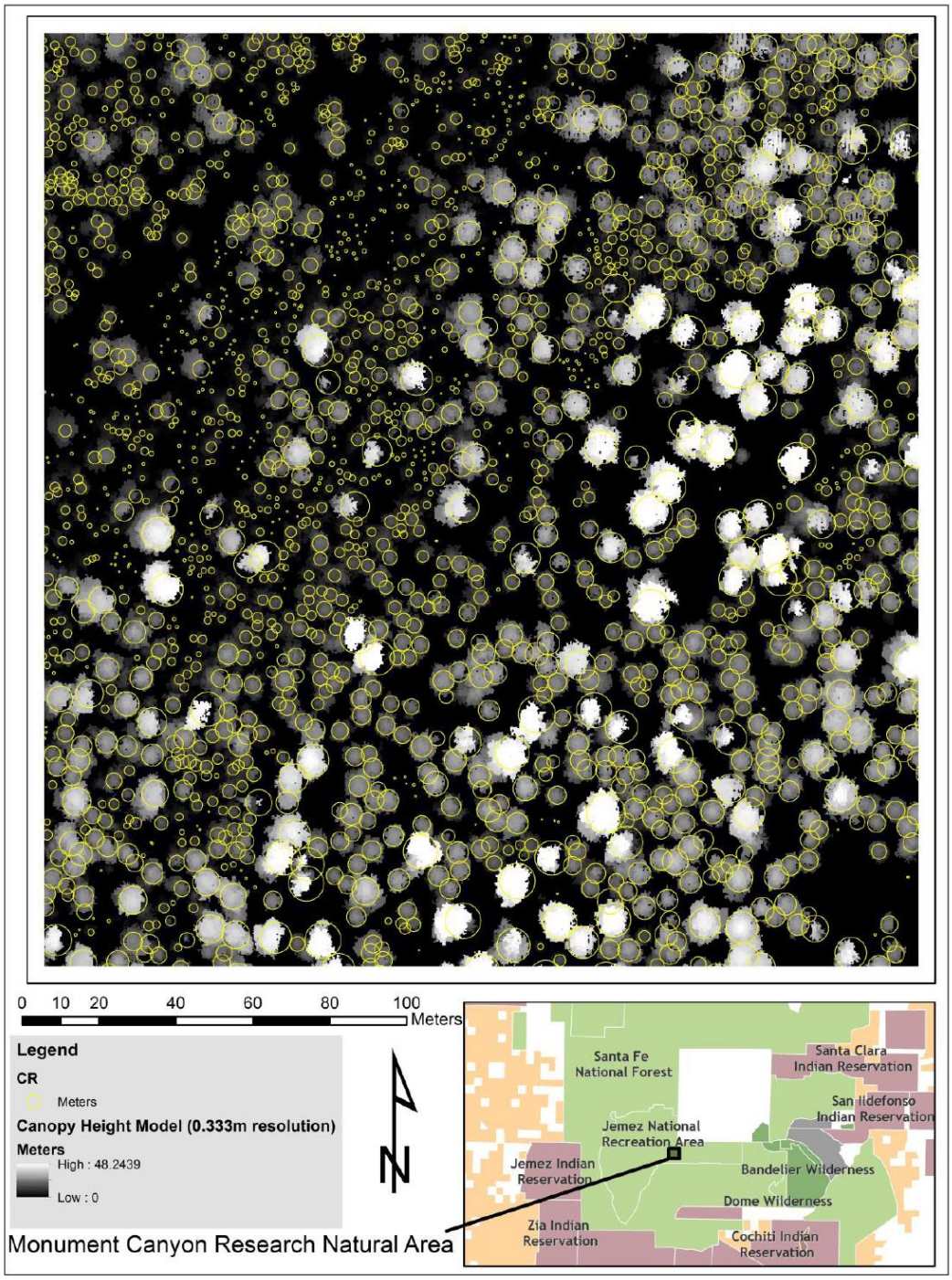

Figure 3. Example of the variable area local maxima (VLM) algorithm output over a section of Monument Canyon, Jemez Mountains, New Mexico (Swetnam and Falk 2014). The canopy height model is 0.333m resolution and is colored from black-to-white for zero height to the tallest height. Individual maxima are shown with the predicted mean-canopy radius (yellow circles) which was used to reduce error of commission about individuals with multiple apical leaders or branches.

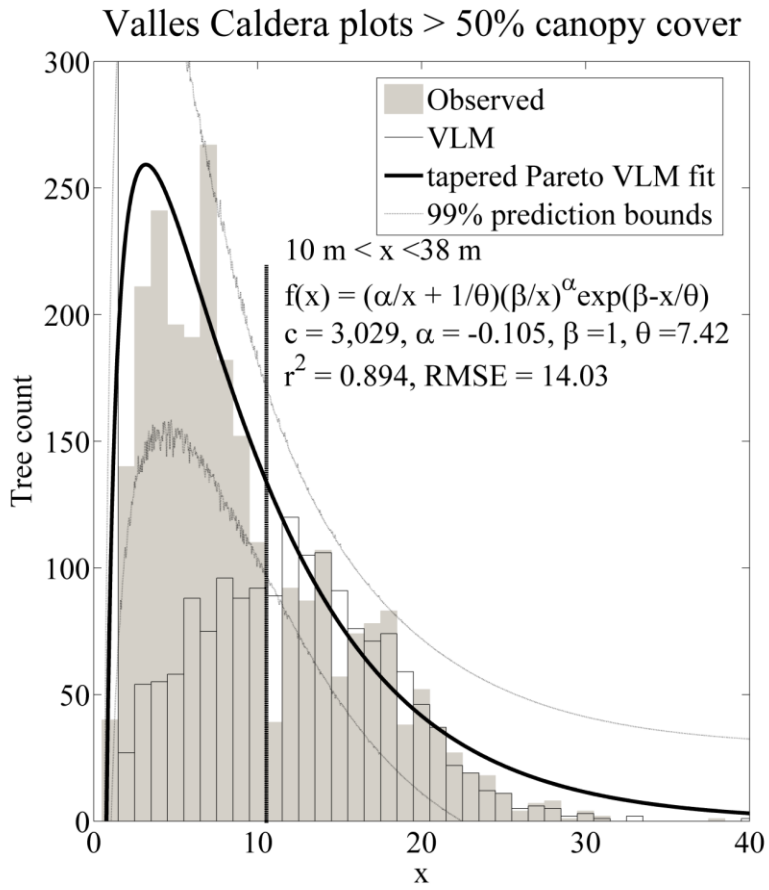

Figure 4. Predicted size-frequency distribution of height (thick black line) based on VLM derived trees (empty black bins) in all plots > 50% canopy cover in the Valles Caldera (gray) (Swetnam et al. in review). The observed frequency of the observed distribution (gray bins) and the tapered Pareto (thick black line) fit using α, θ, and c determined by least squares regression, the β parameter was set at 1 m height. A > 10 m cut-off height for the VLM was used to fit the function (vertical dashed line) due to increasing error of omission in understory. Histogram has 1 m width linear bins.

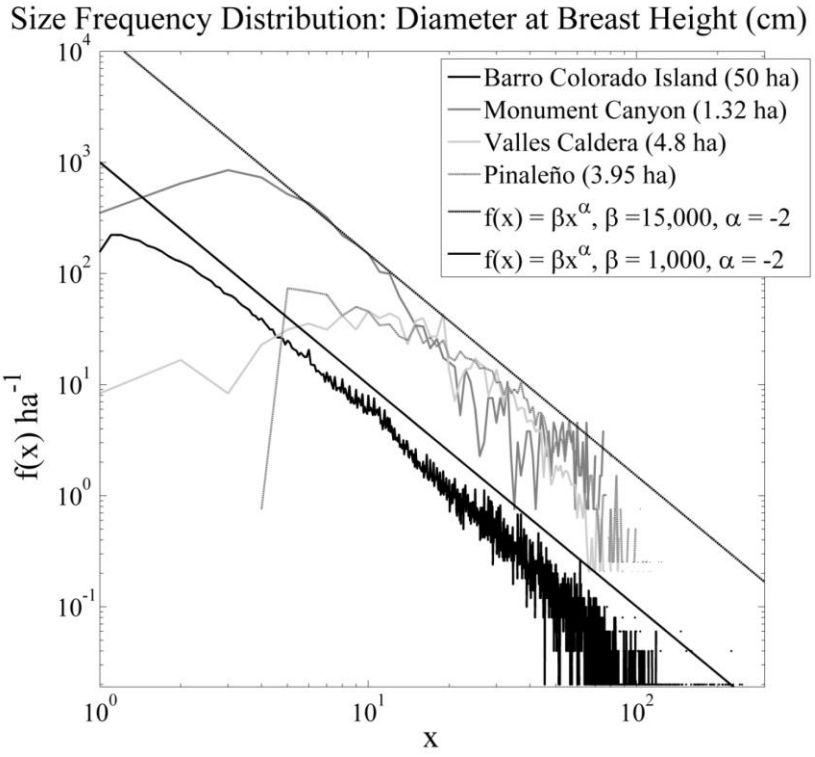

Figure 5. Scaling of size frequency distribution in semi-arid vs tropical forest (Swetnam et al. in review). Size distribution for tree diameter [in 1cm wide linear bins] from the data in four study areas normalized to represent the frequency of trees per hectare $f(x)\ ha^{-1}$. Two reference lines have -2 slope, predicted by the MST for tree diameter.

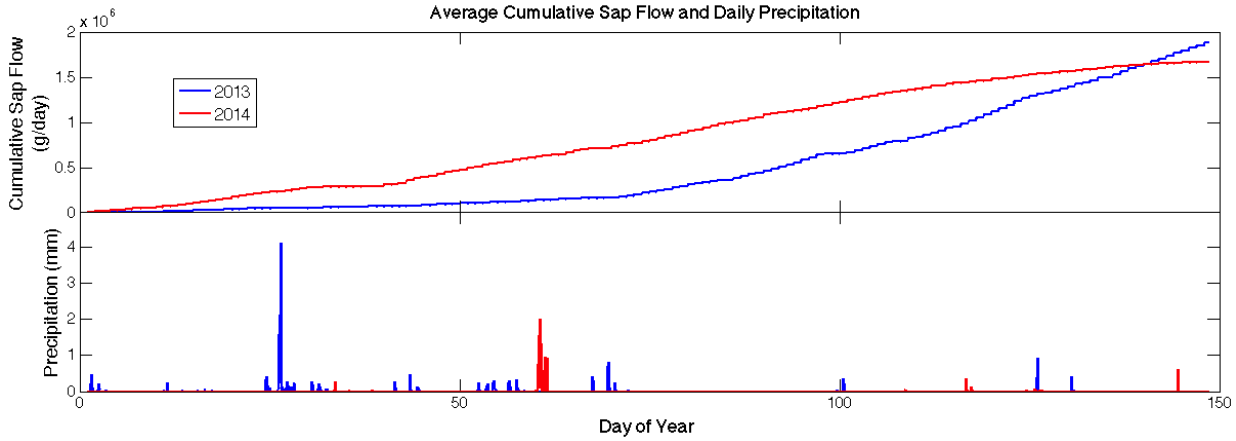

Figure 6. Multi-year comparisons of sap flux under different climatic regimes in SCM (Barron-Gafford et al.).

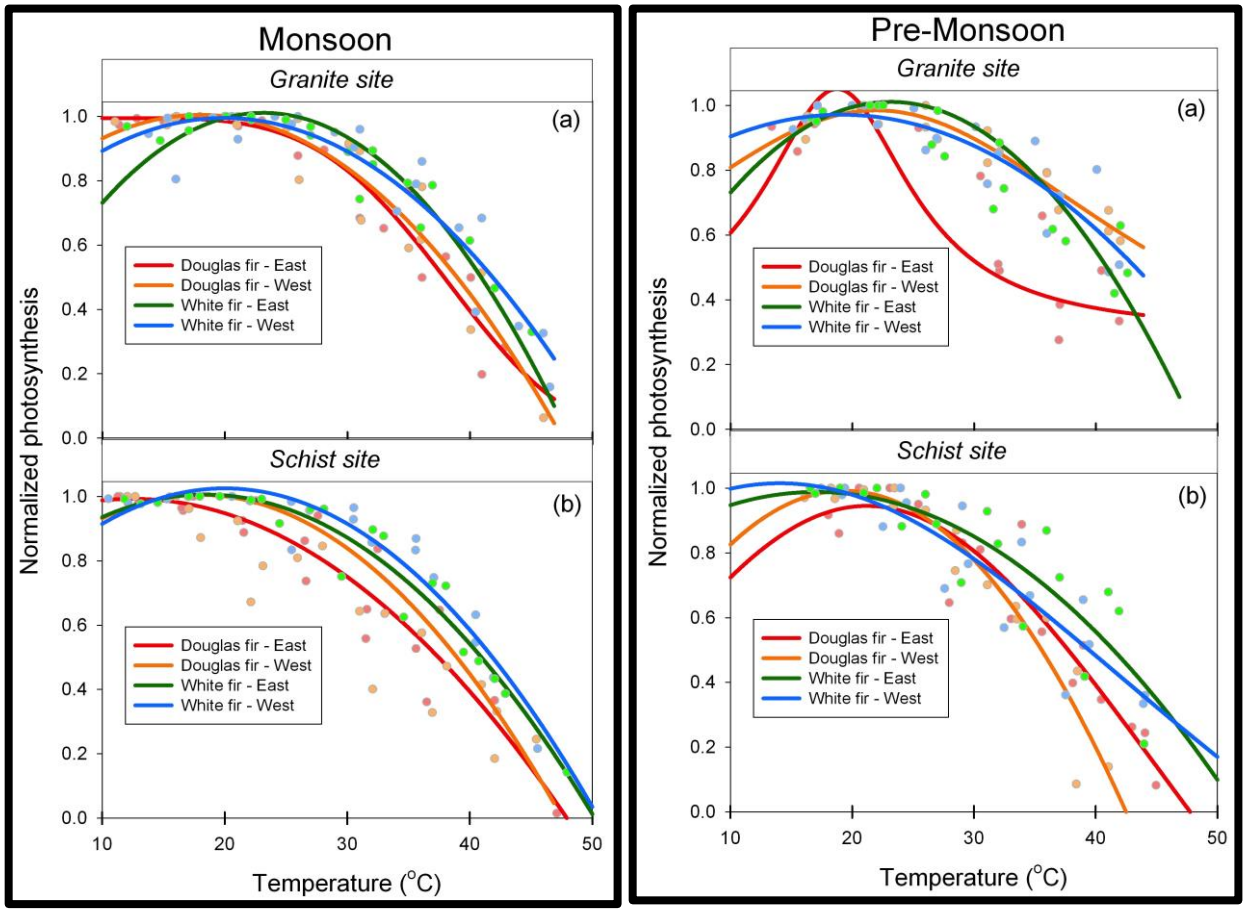

Figure 7. Trees in demonstrated augmented function under monsoon augmented soil moisture, with trees on schist showing greater effect than trees on granite, highlighting the importance of lithology. (Barron-Gafford et al.)

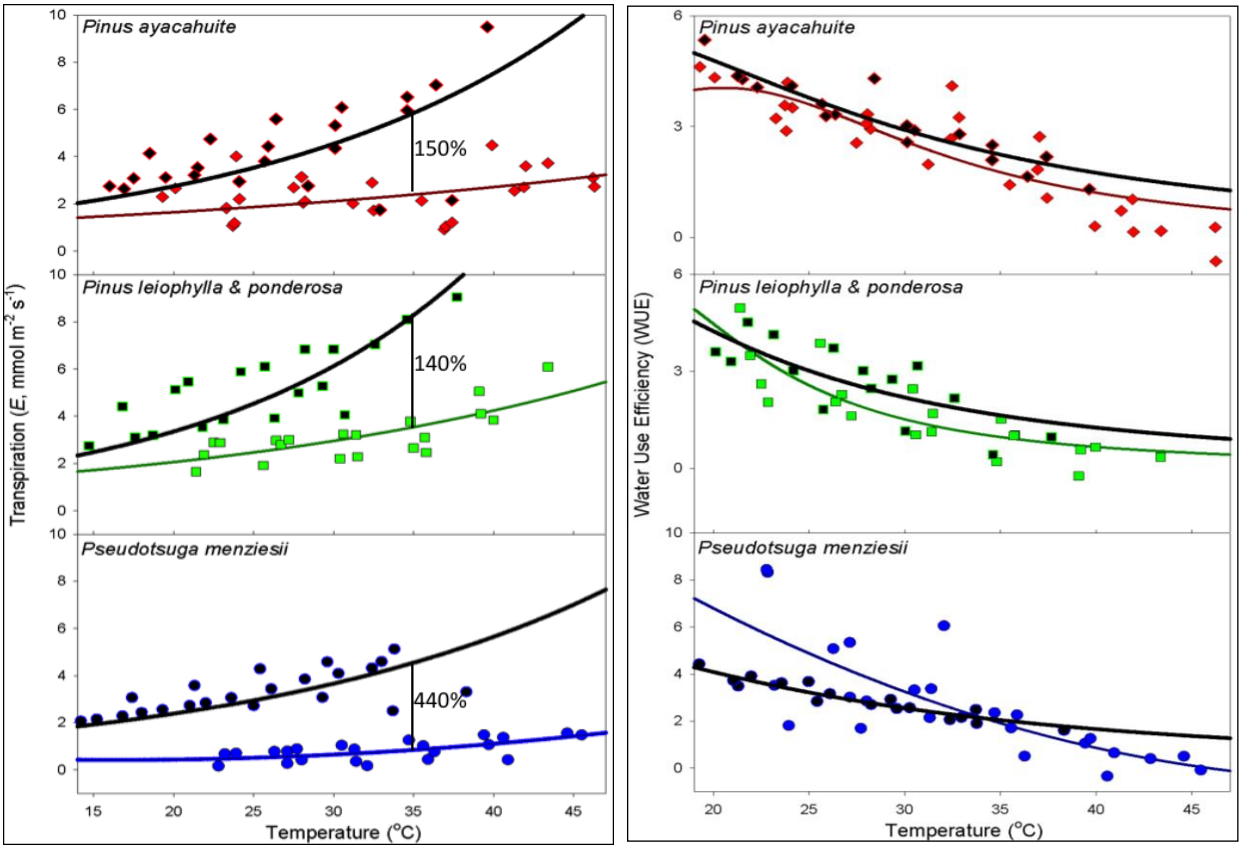

Figure 8. Transpirational water loss increased significantly due to the onset of the summer monsoon rainy season, as expected, but there were dramatic differences in the responsiveness of species to this renewed water resource (light symbols represent pre-monsoon, darker symbols represent data from the monsoon period). *P. menziessii* showed the biggest response indicating severe water stress during the summer dry period. In terms of water use efficiency (WUE; carbon uptake per unit water loss), all *Pinus* species were similar in their degree of WUE among one another and across seasonal periods of variable moisture, indicating a tight coupling between water use and carbon uptake. Again, *P. menziessii* showed a very different pattern with WUE actually being lower at most temperatures that the trees experienced, indicating high rates of water loss per unit carbon assimilation. (Data from Barron-Gafford et al.)

Table 1. JRB Las Conchas burn phenocam locations and observations (Papuga et al.)

Camera	Aspect	Elevation	Grass?	Herbs?	Aspens?
1	East-Facing	High	Some	Yes	**No**
2	East-Facing	Middle	Yes	Yes	Very few
3	East-Facing	Low	Yes	Yes	Yes
4	West-Facing	High	Yes	Yes	Yes
5	West-Facing	Middle	Yes	Yes	Yes
6	West-Facing	Low	Yes	Yes	Yes
7	East-Facing	High	Some	Yes	**No**
8	East-Facing	Low	Yes	Some	Yes
9	West-Facing	High	Yes	Yes	Yes
10	West-Facing	Low	Some	Yes	Yes

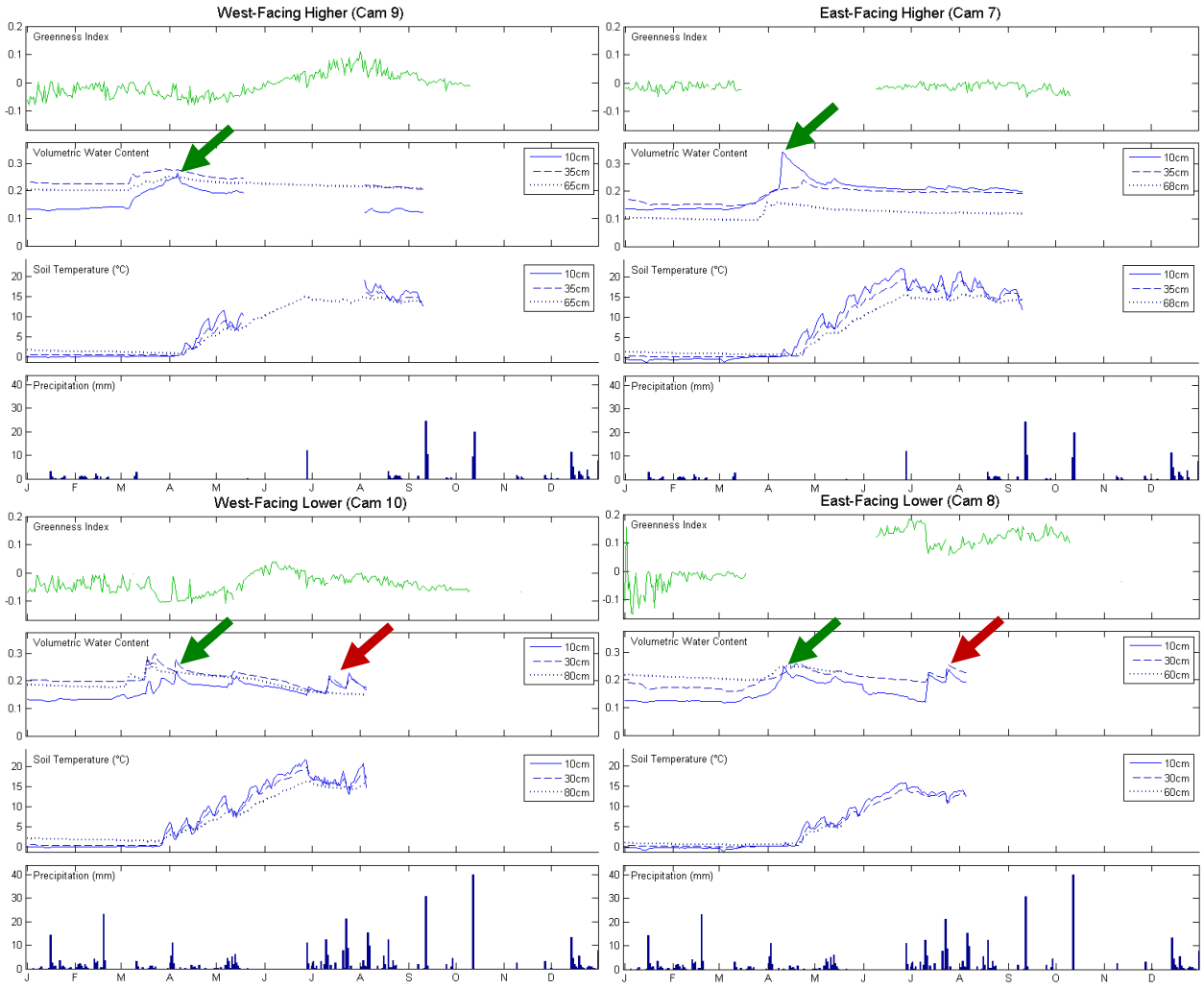

Figure 9. Post-burn understory dynamics following the Las Conchas wildfire (July 2011) show phenocam-derived greenness is related to aspect-variable soil moisture conditions (Papuga et al.).

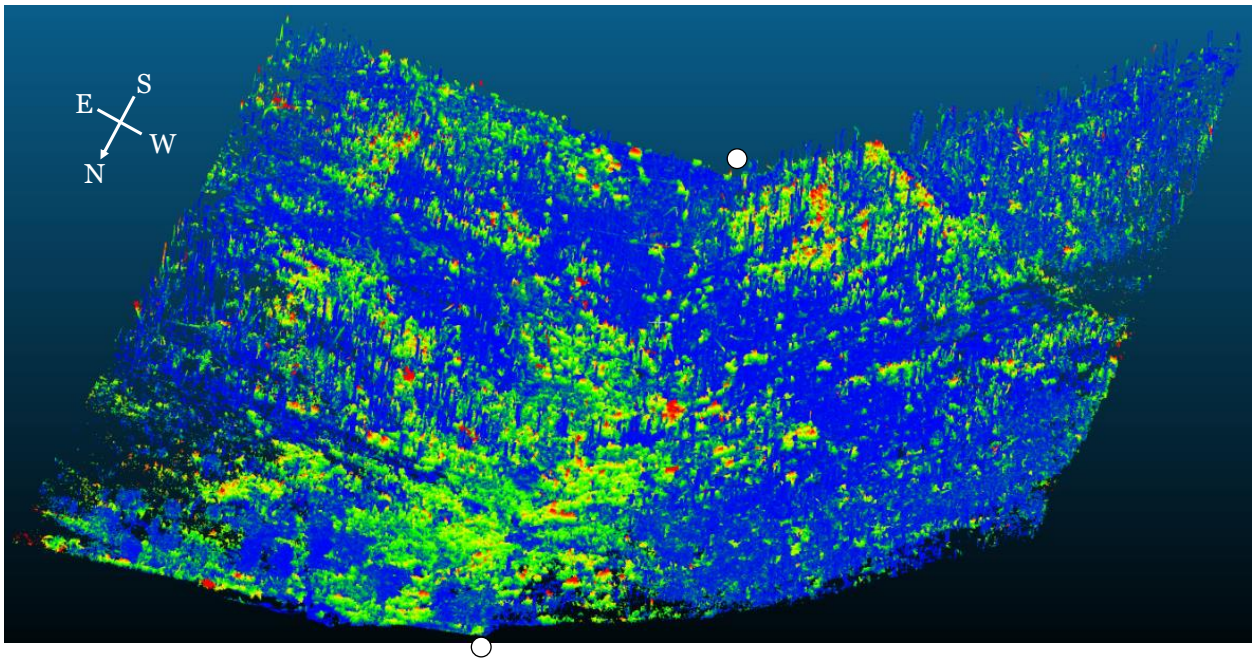

Figure 10. Four terrestrial LiDAR scans of one of the watersheds were performed between Sept 2011 and May 2013. Comparing two different point clouds allows visualization of landscape changes at every point in the cloud (Papuga et al.).

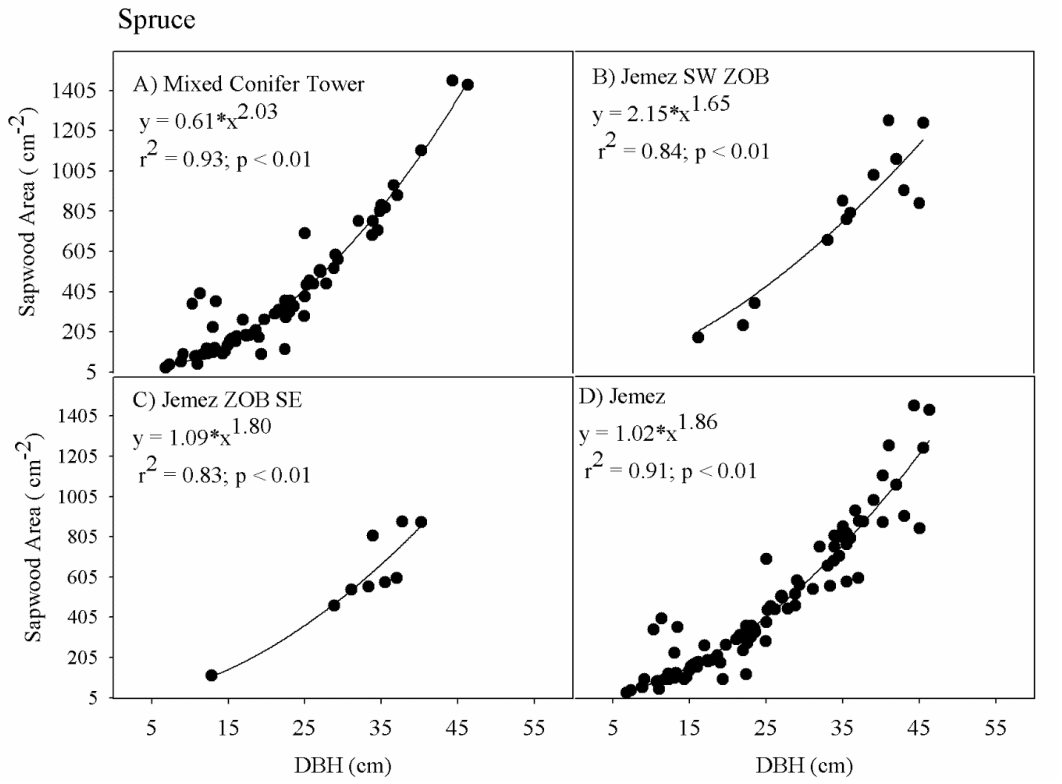
Spruce
A) Mixed Conifer Tower
y = 0.61*x^2.03
r^2 = 0.93; p < 0.01
B) Jemez SW ZOB
y = 2.15*x^1.65
r^2 = 0.84; p < 0.01
C) Jemez ZOB SE
y = 1.09*x^1.80
r^2 = 0.83; p < 0.01
D) Jemez
y = 1.02*x^1.86
r^2 = 0.91; p < 0.01
Sapwood Area (cm-2)
DBH (cm)

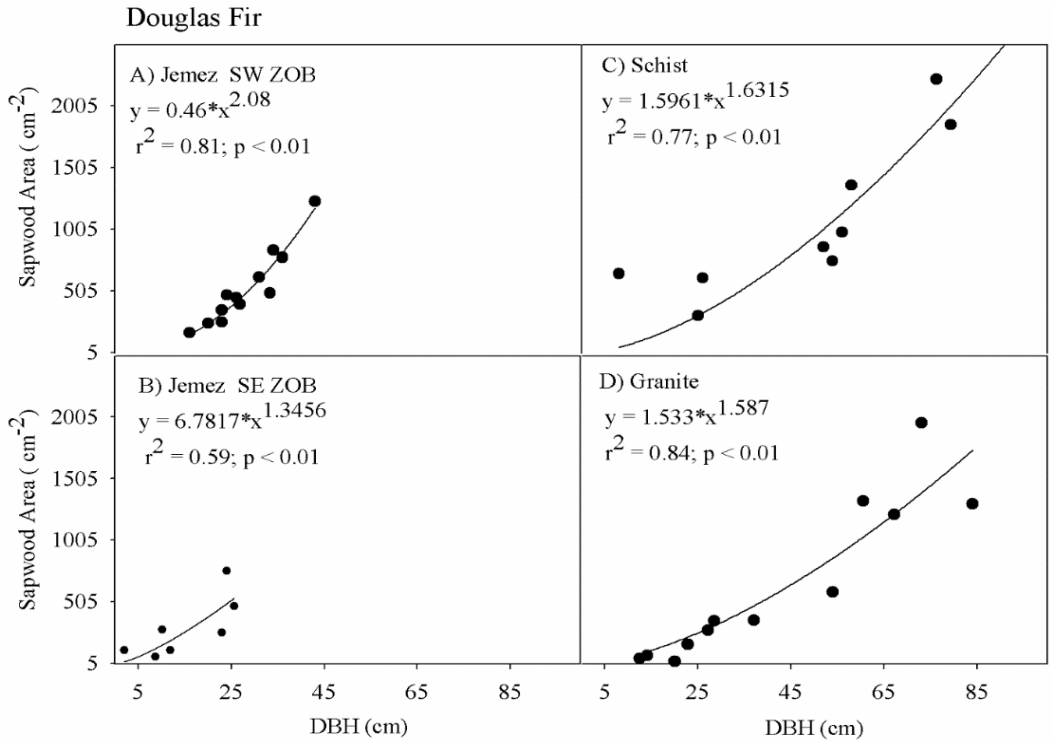
Douglas Fir
A) Jemez SW ZOB
y = 0.46*x^2.08
r^2 = 0.81; p < 0.01
C) Schist
y = 1.5961*x^1.6315
r^2 = 0.77; p < 0.01
B) Jemez SE ZOB
y = 6.7817*x^1.3456
r^2 = 0.59; p < 0.01
D) Granite
y = 1.533*x^1.587
r^2 = 0.84; p < 0.01
Sapwood Area (cm-2)
DBH (cm)

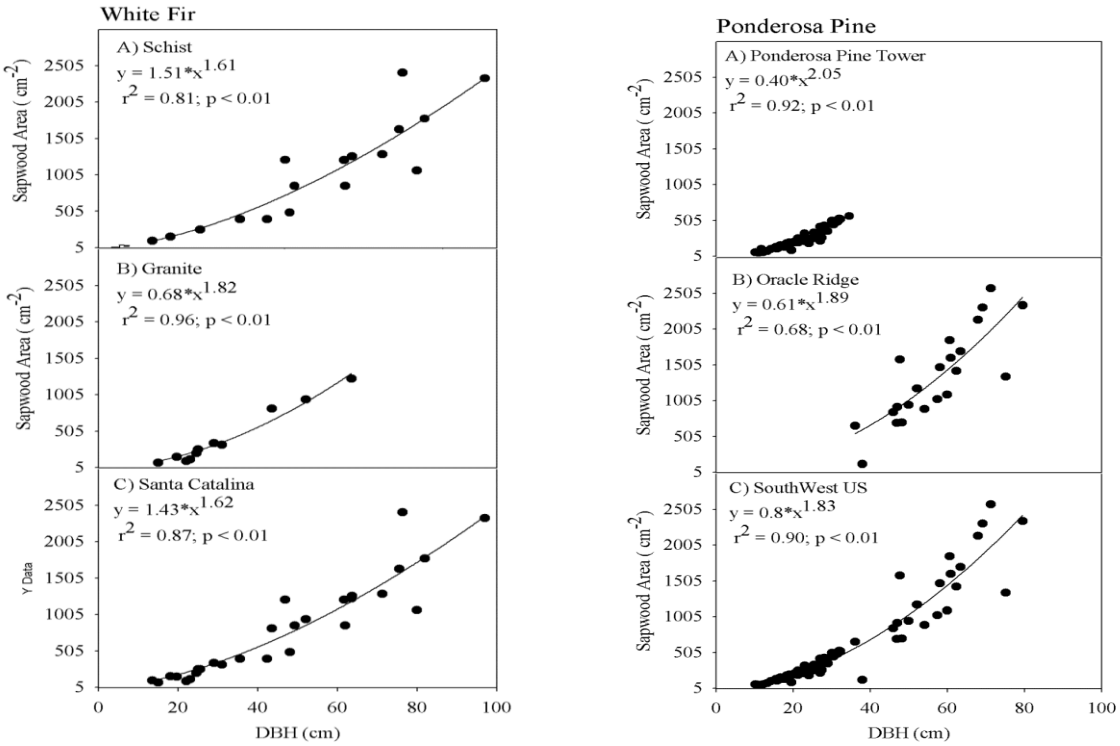

Figure 11. Allometric relationships are established on the basis of primary size measures [diameter at breast height (DBH), canopy diameter (CD) and tree height (H)] to predict sapwood cross sectional area (As) because direct observation of sapwood is impossible without damaging the tree. Allometric relationships vary by tree species thereby requiring unique correlation coefficients and scaling exponents. While species-specific allometric relationships have been established in the literature, it is unclear whether these relationships are influenced by first order effects such as aspect, elevation or soil texture. The goal of this research is to determine whether allometric relationships are generalizable across sites with similar species but different parent materials, slopes, and aspects. To do this, we analyzed the allometric relationship of co-occurring deciduous and evergreen vegetation across two high and mid elevation mixed forest ecosystem in New Mexico and Arizona. The allometric relationship can be generalized for some species (white fir and spruce) while site specific equations may be required for Douglas fir. Mountain topography can create heterogeneity in transpiration trends on account of variation in precipitation, soil moisture and atmospheric conditions. However, a generalized allometric equation eliminates logistical challenge in obtaining allometric equations across an elevation gradient and thereby simplifies transpiration estimate across space and time.

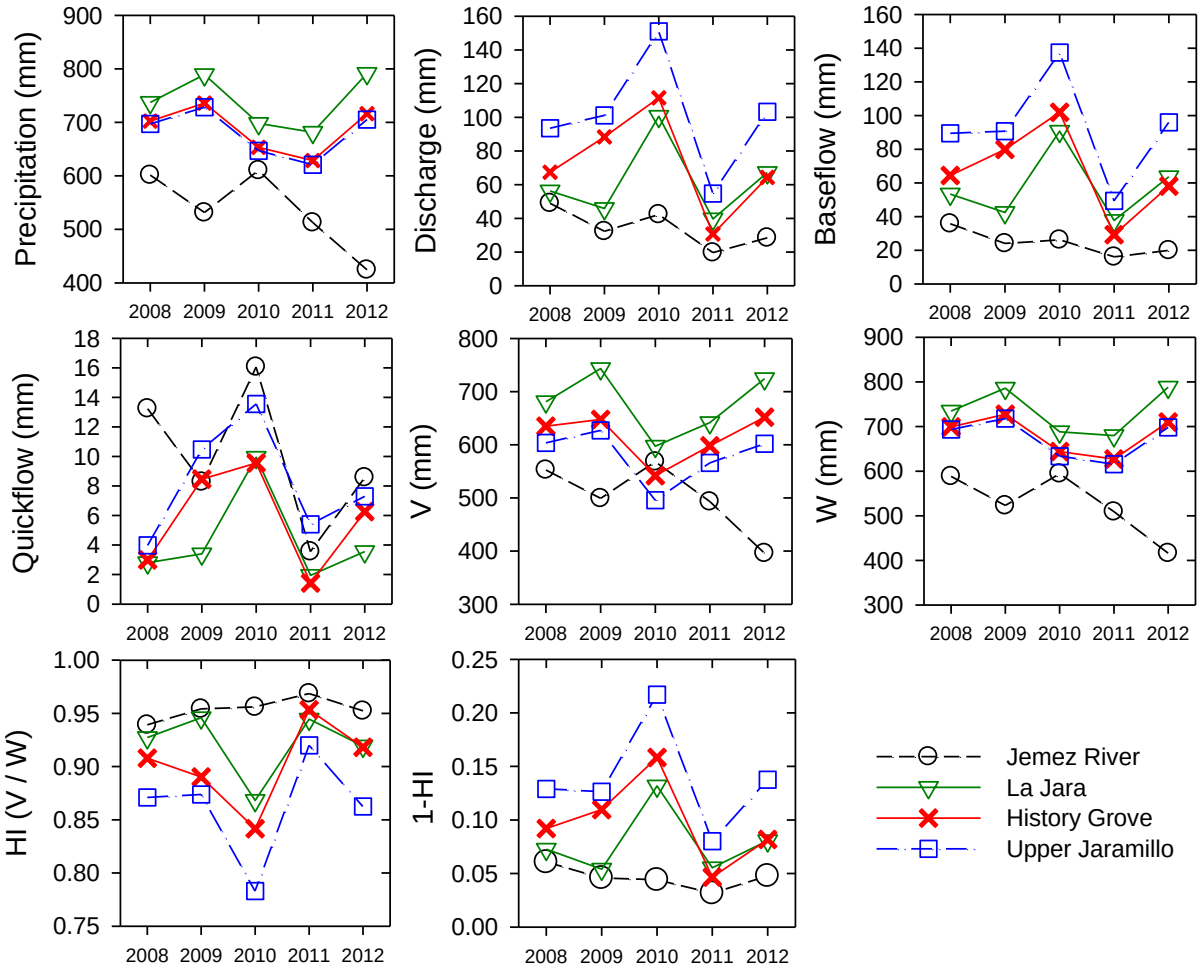

Figure 12. Hydrological partitioning of the Jemez River and high elevation catchments characterized by a different predominant aspect (La Jara, History Grove and Upper Jaramillo) during 5 water years 2008 to 2012 (Zapata-Rios et al.)

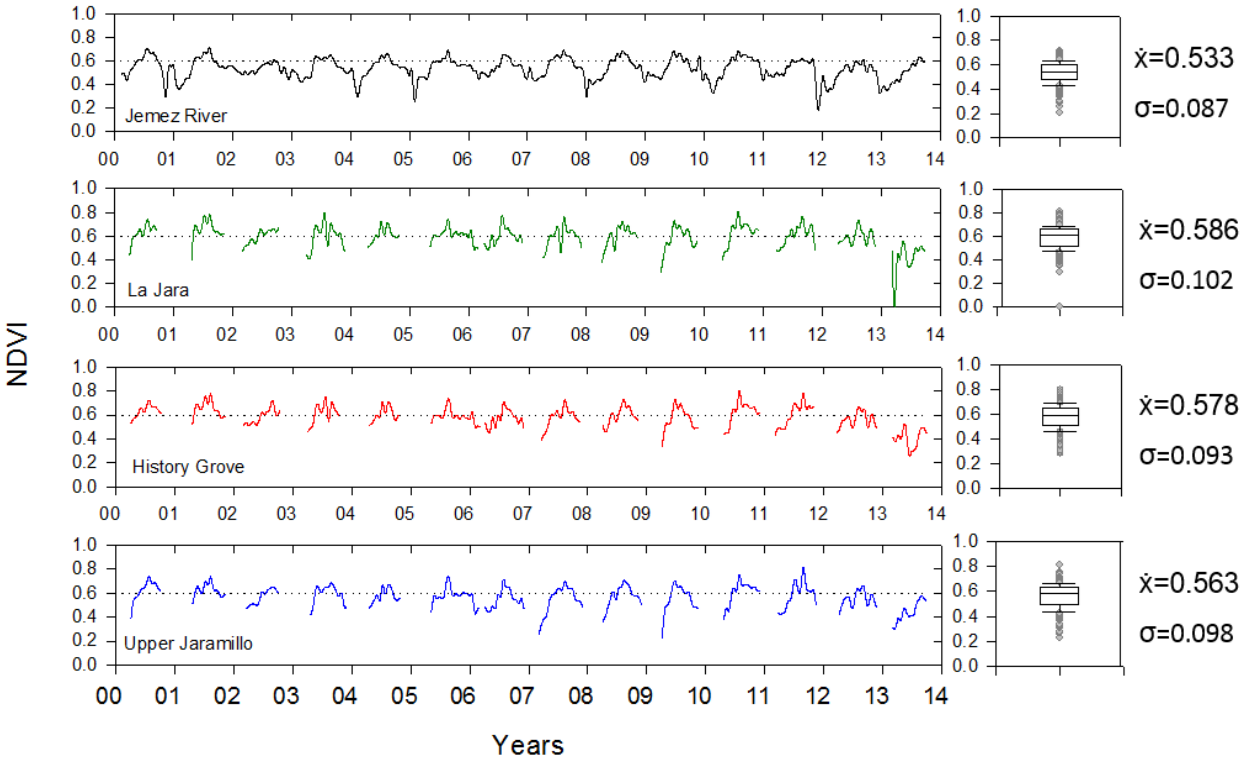

Figure 13. 14-years series of Normalized Difference Vegetation Index (NDVI) in the Jemez River and 1st order high elevation catchments derived from NASA's Moderate Resolution Imaging Spectroradiometer (MODIS) Land Products MOD13A2 with a spatial resolution of 250 m (Zapata-Rios et al.).

Table 2. Area under NDVI curve and above 0.60

	Jemez	La Jara	History Grove	Upper Jaramillo
Average	0.2	0.48	0.41	0.34
stdev	0.13	0.17	0.19	0.15
c.v.	0.63	0.34	0.45	0.45

Table 3. Number of days above a NDVI = 0.6

	Jemez	La Jara	History Grove	Upper Jaramillo
Average	91	148	116	110
stdev	40	25	38	42
c.v.	0.44	0.17	0.33	0.39

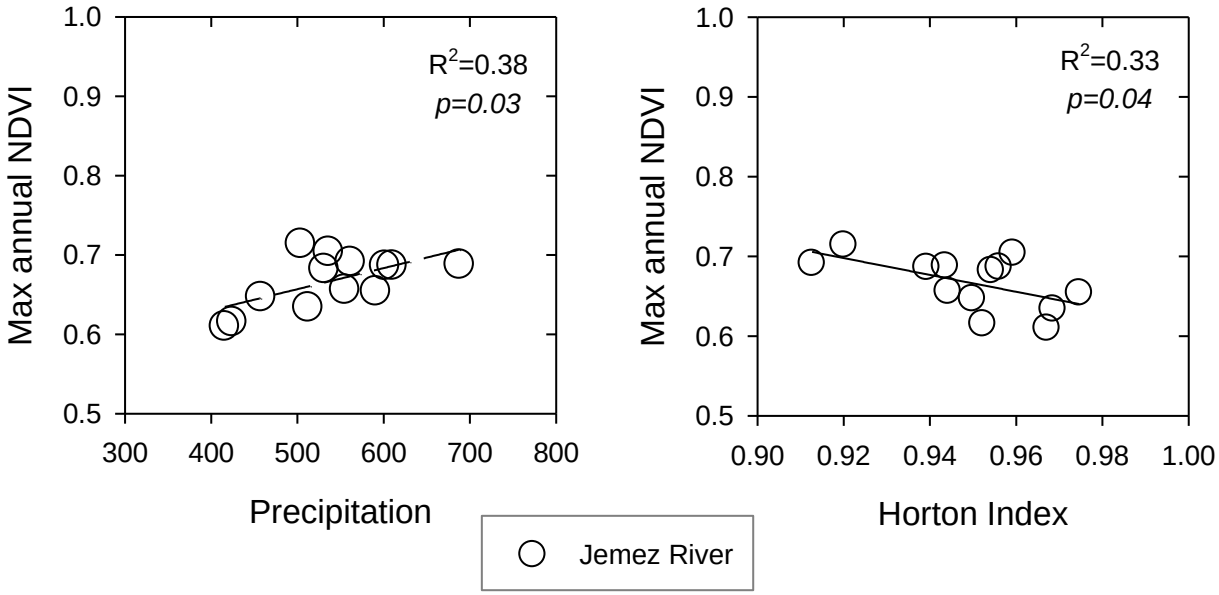

Figure 14. Maximum annual NDVI versus precipitation and Horton Index for the Jemez River Basin (Zapata-Rios et al.).

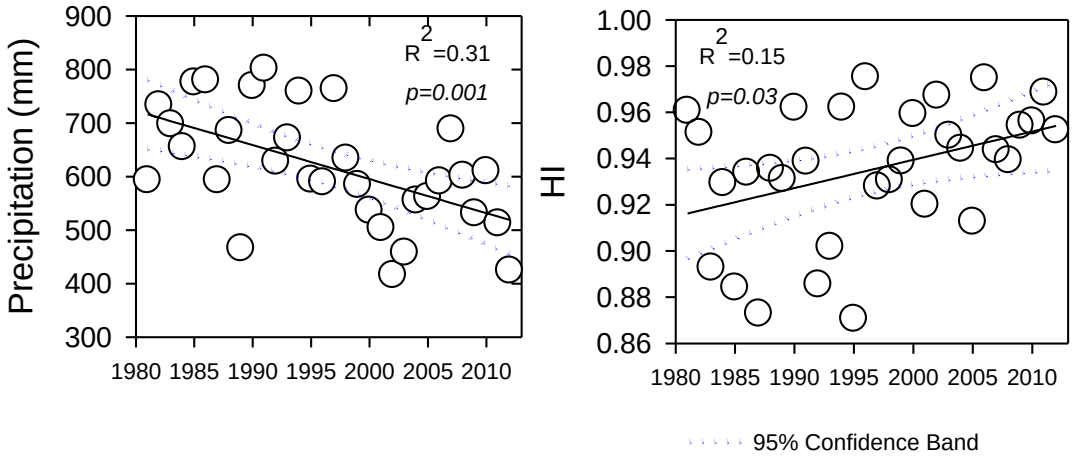

Figure 15. Long term total precipitation and Horton Index variability in the Jemez River Basin (Zapata-Rios et al.).

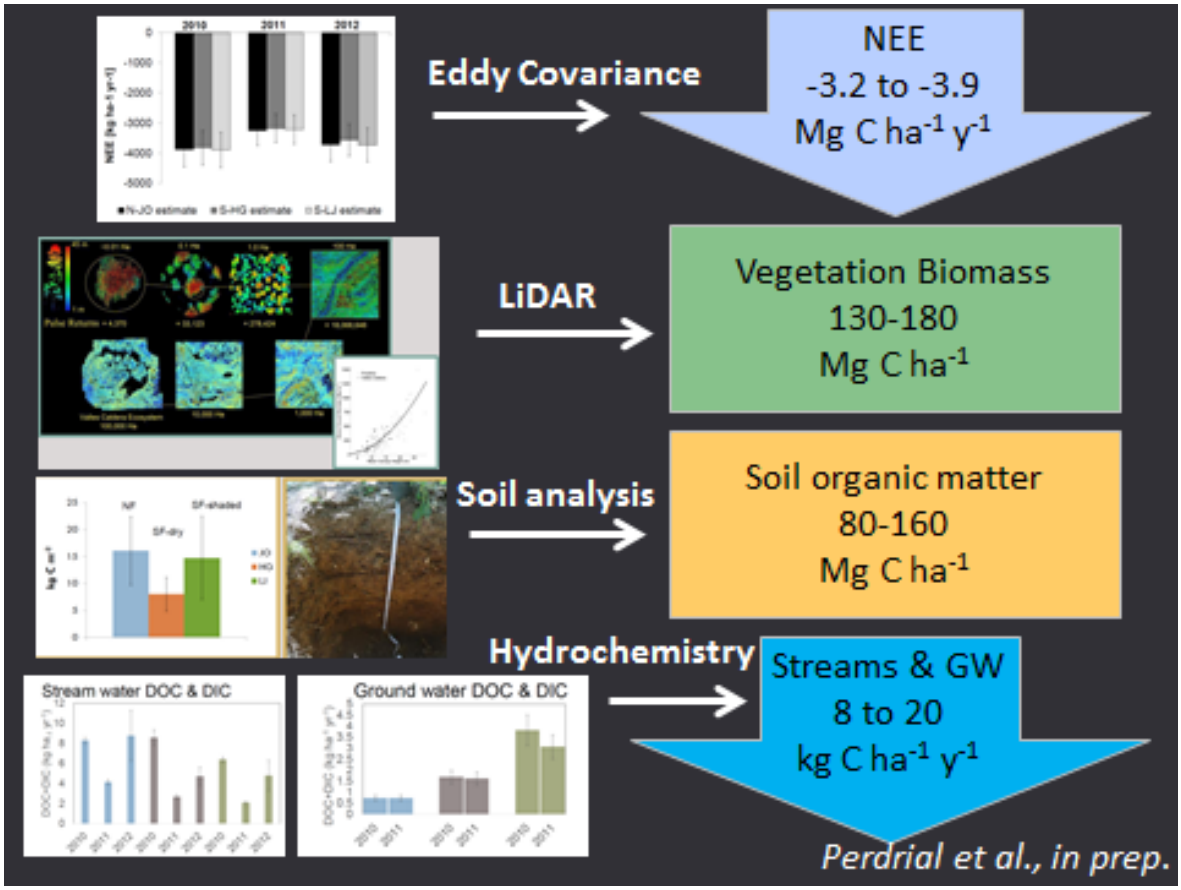

Figure 16. Pre-burn mass balance of carbon measured over a three year period for three JRB CZO headwater catchments (La Jara, History Grove, and Upper Jaramillo) using a combination of eddy covariance (distributed model), LiDAR, soil analysis and streamwater hydrochemistry and flux (Perdrial, Swetnam et al., in prep.).

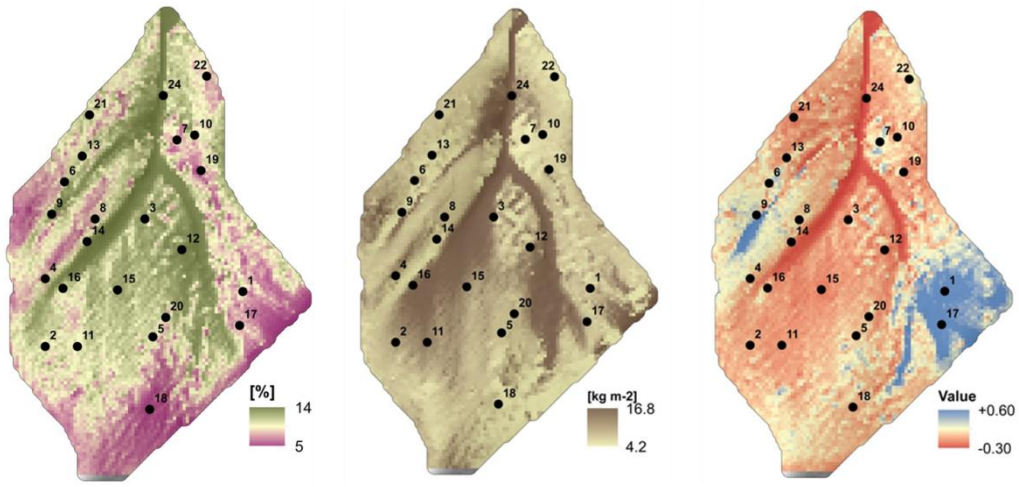

Figure 17. Predicted spatial variation in percent clay, carbon stocks, and Na depletion/ enrichment across a ~6 ha granitic ZOB in the SCM (Holleran et al., in review).

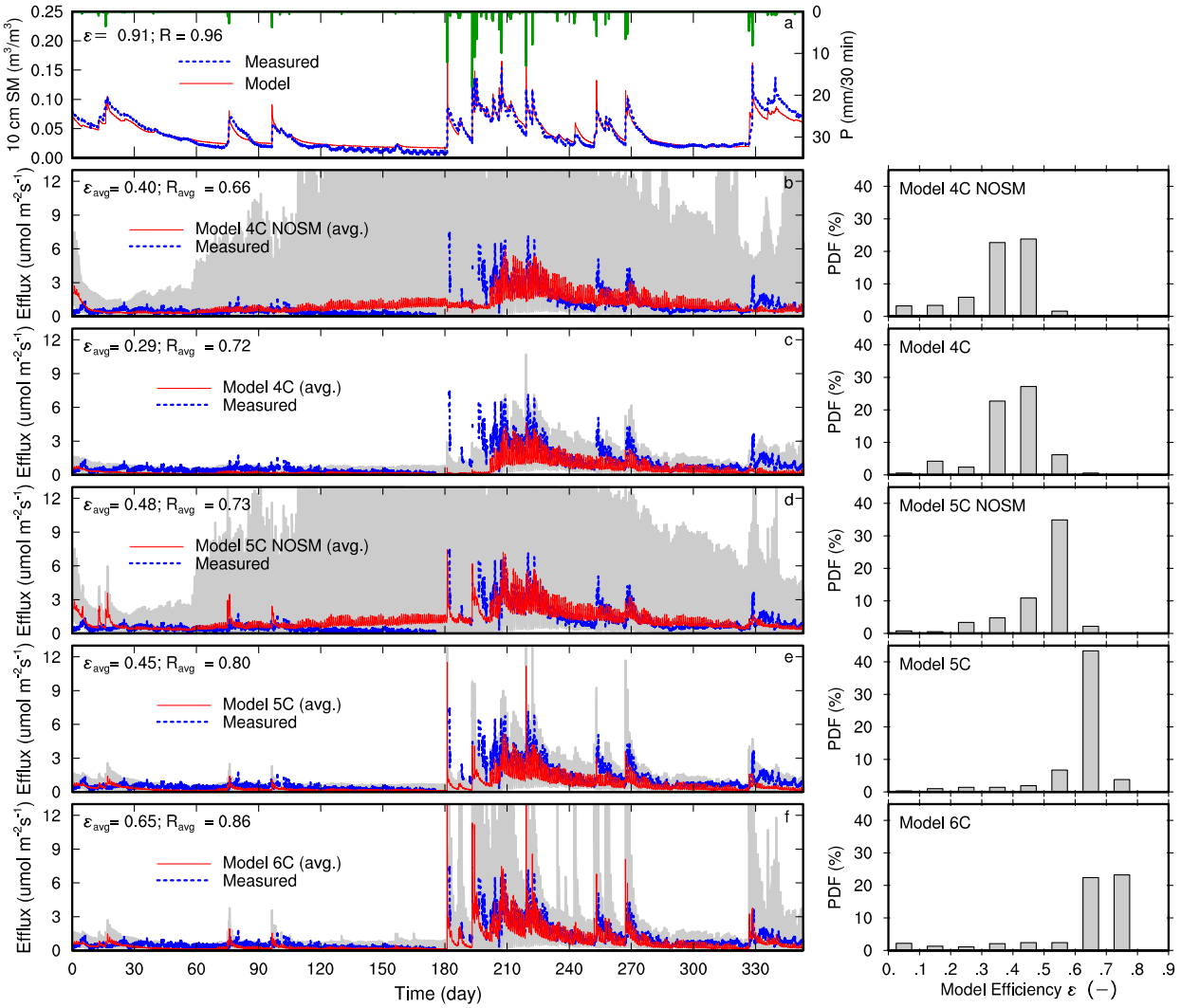

Figure 18. Comparison of the modeled (red lines) to the observed (dashed blue lines). (Left panels) Volumetric soil moisture (in $m^3\ m^{-3}$) at 10 cm (a), CO_2 efflux at the soil surface (in $\mu mol\ m^{-2}\ s^{-1}$) modeled by a 4-carbon pool model without (b) and with (c) explicit soil moisture control, by a 5-carbon pool model without (d) and with (e) soil moisture control, and a 6-carbon pool model with soil moisture control (f). The shaded area represents the upper and lower bounds of 625 ensembles resulting from combinations of uncertain parameters. Precipitation (in mm / 30 min; green lines) is also included in (a). In the legend ε stands for the Nash–Sutcliffe model efficiency and r for correlation coefficient. (Right panels) Probability density function (PDF) of best simulations for the five evolving models (the 6-carbon pool model produces a greater number of best simulations with greater ε values) (Niu et al.).

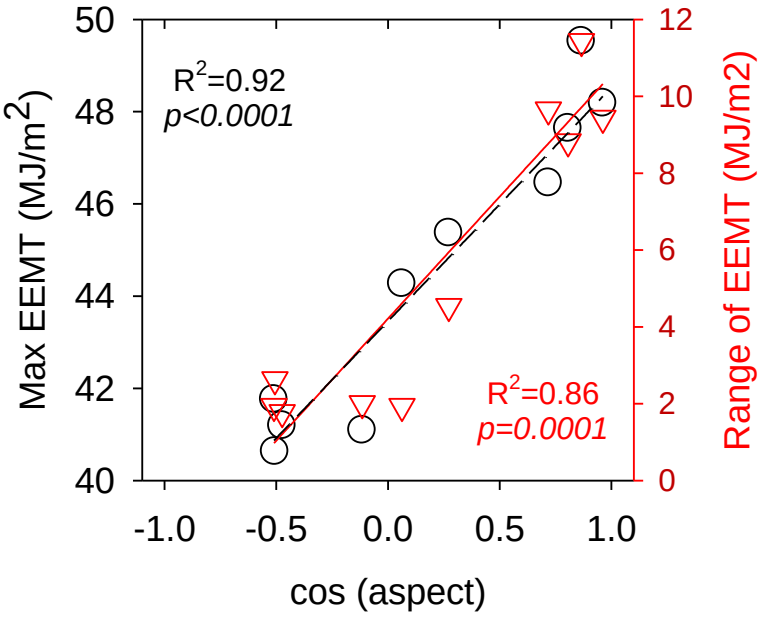

Figure 19. Maximum EETM versus mean aspect within JRB springs' contributing areas (Zapata-Rios et al.).

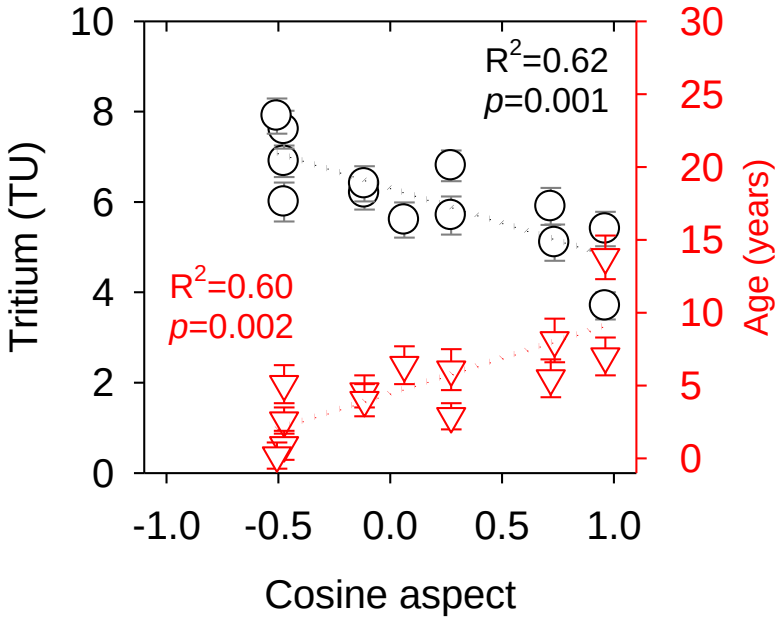

Figure 20. Tritium concentrations and age versus mean aspect within JRB springs' contributing areas (Zapata-Rios et al.)..

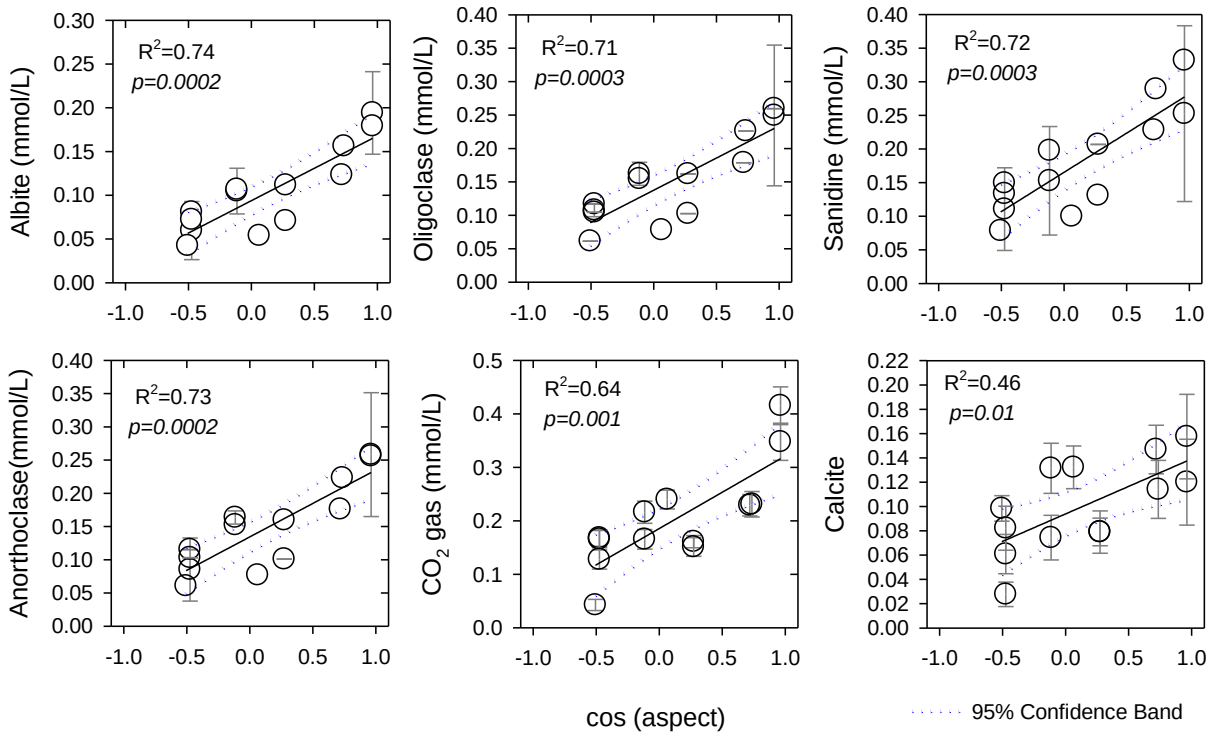

Figure 21. Mineral fluxes estimated with Netpath at the JRB springs versus mean aspect (Zapata-Rios et al.)..

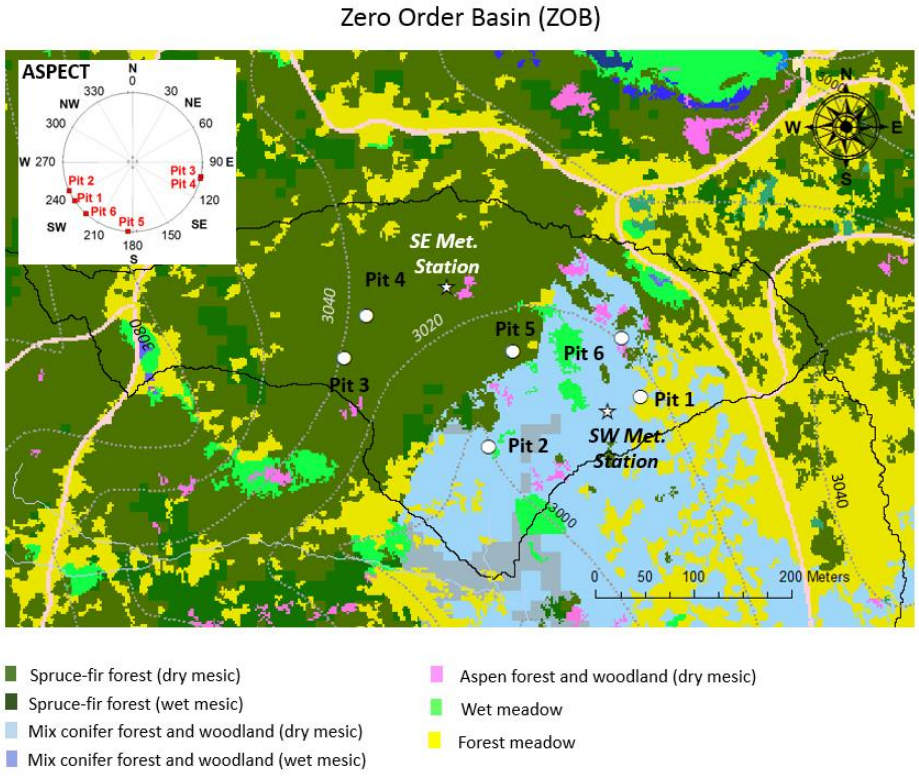

Figure 22. Vegetation transition in the JRB ZOB, location and aspect of pedons.

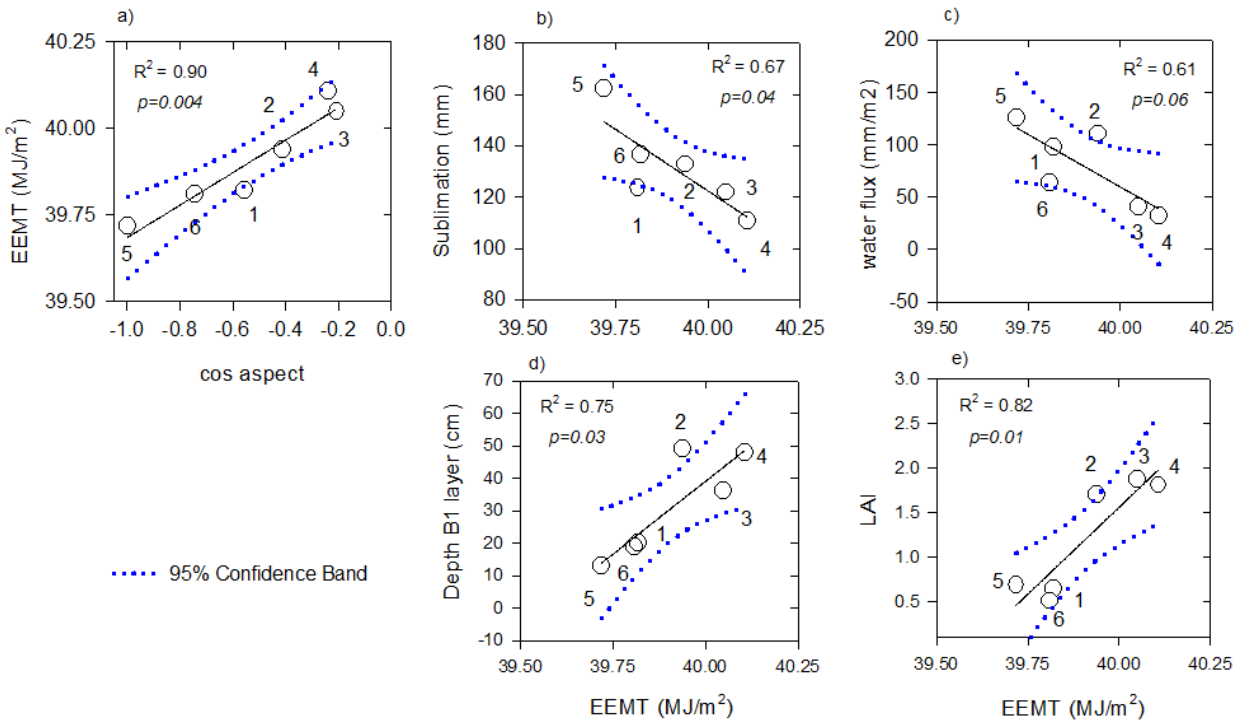

Figure 23. Energy, water fluxes, soil and vegetation response in 6 instrumented pedons in the JRB ZOB. Total water lost by sublimation was estimated with SnowPALM between Oct 2010 and Sep 2012. Water fluxes is the total amount of water between March 2011 and September 2012 registered by the wick lysimeters at the shallow depth approx ~ 5cm (Zapata-Rios et al.)..

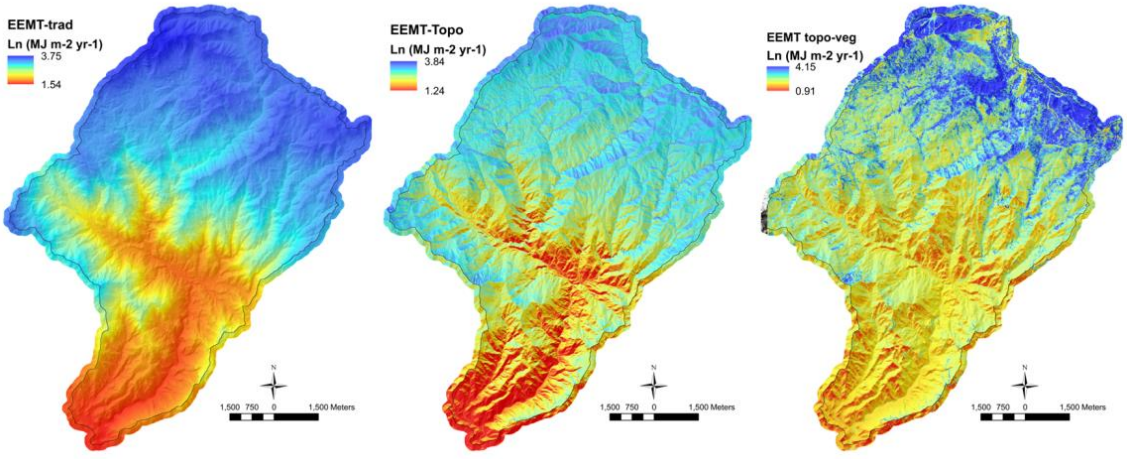

Figure 24. Predicted rates of EEMT for Sabino Canyon Watershed (SCM) based on the traditional method of EEMT calculation, the topographically modified EEMT, and EEMT that accounts for both topography and the current vegetation structure (Rasmussen et al.).

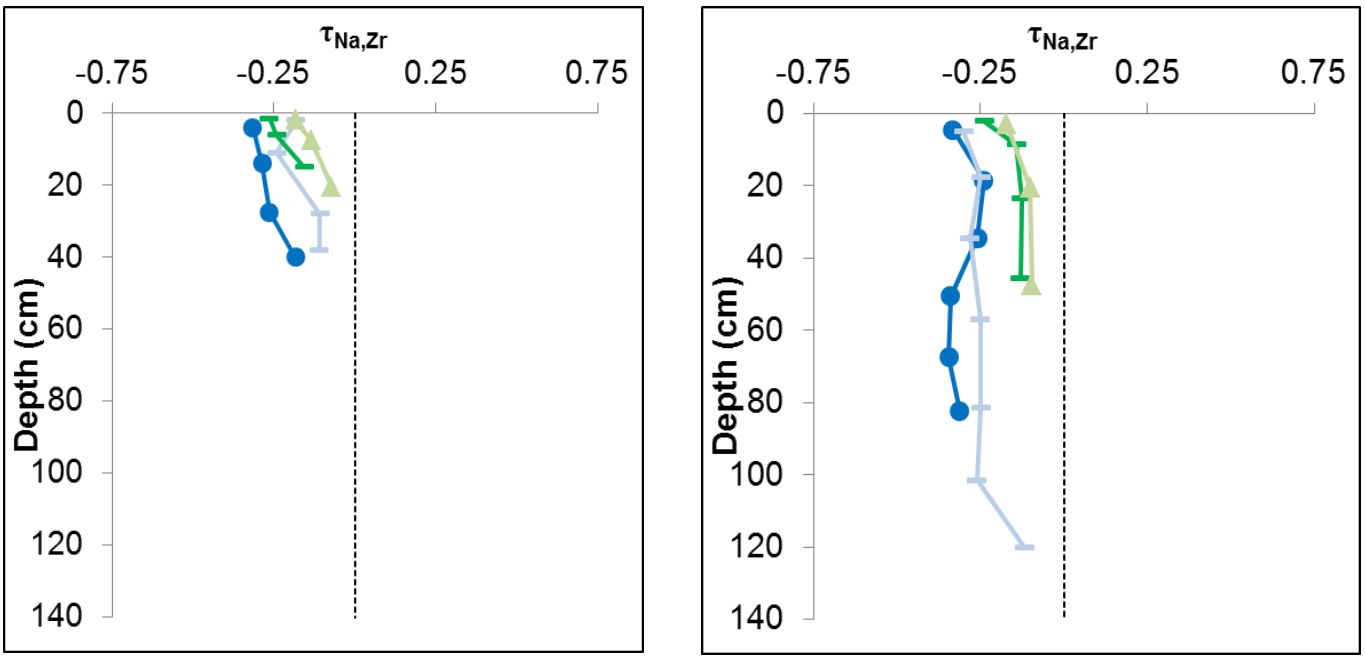

Figure 25. The relative depletion of Na in bulk soils for convergent (blue) and divergent (green) landscape positions the desert scrub (dry) and mixed conifer (wet) locations on the SCM elevation gradient (Lybrand et al.).

Mixed Conifer						
	% Total Soil C		C:N		$\Delta^{14}C$	
	Convergent	Divergent	Convergent	Divergent	Convergent	Divergent
Free Light Fraction	23	51	36	35	10	98
Occluded	21	9	40	39	-3	-2
Mineral	57	39	20	17	26	38

Table 4. The distribution, C:N, and radiocarbon content of C in density and aggregate fractions in the mixed conifer location.

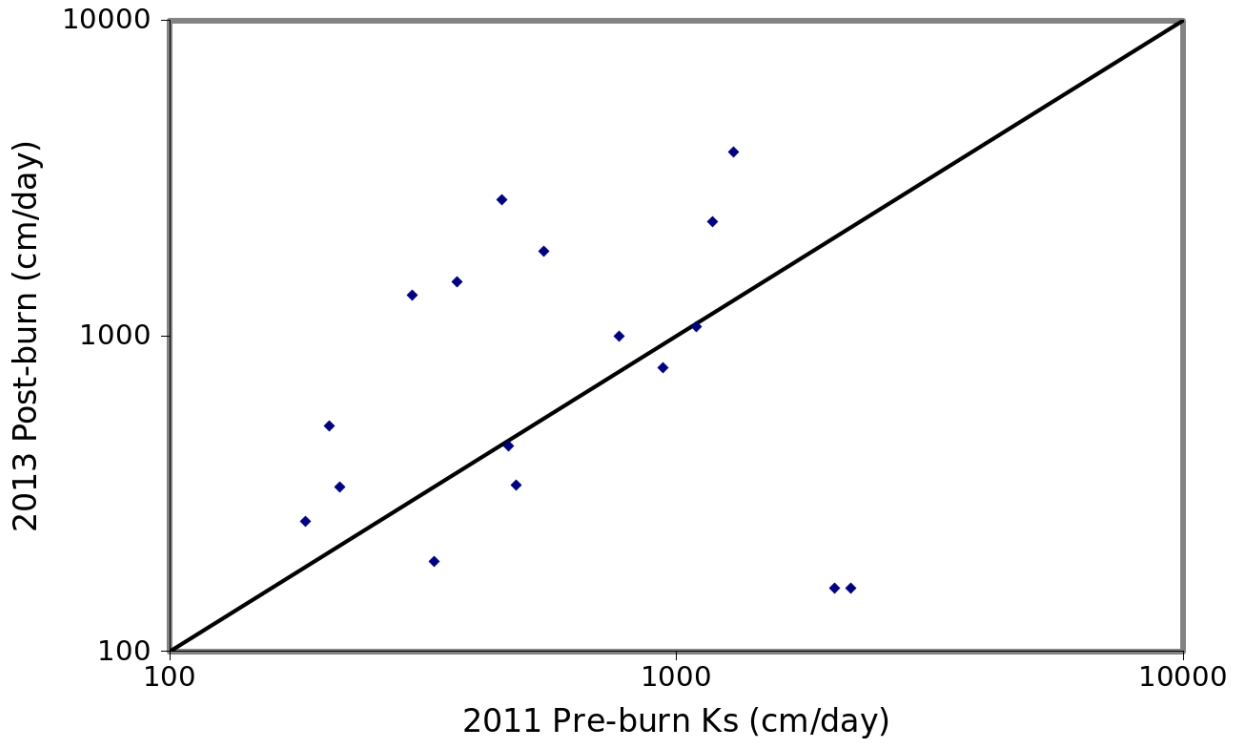

Figure 26. Pre and post burn saturated hydraulic conductivities of the mineral soil at 17 precisely geo-referenced locations within the Valles-Caldera, La Jara catchment mixed conifer zero-order-basin (Kopp et al.).

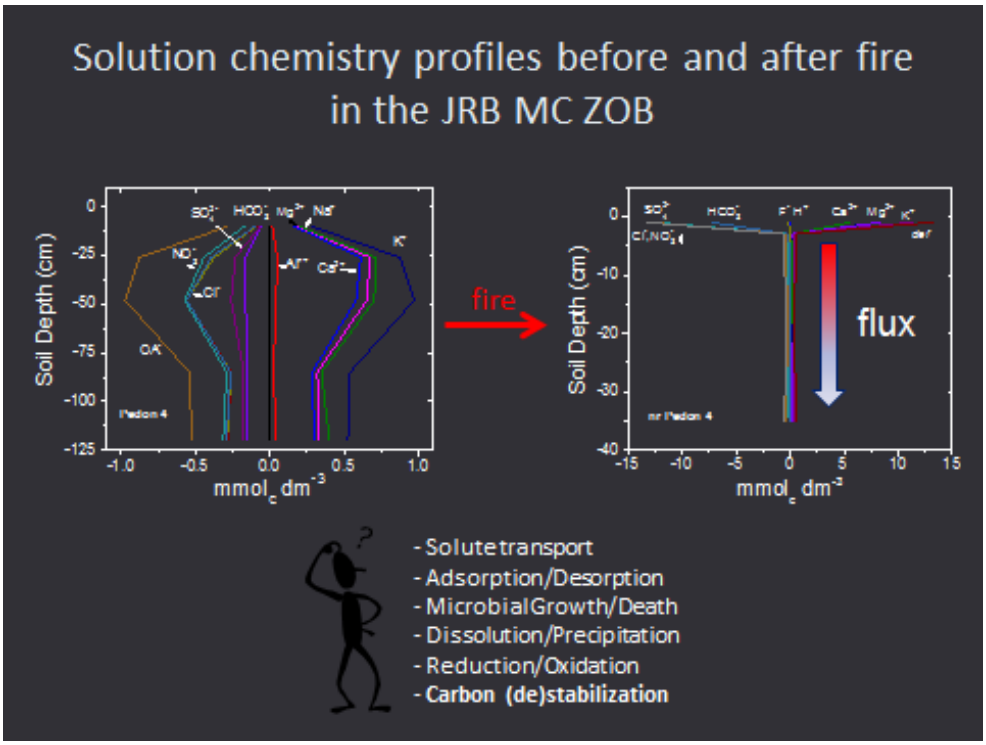

Figure 27. Solution chemistry profile for Pedon 2 in the JRB MC ZOB before and after fire show a large increase in soluble lithogenic ions whose propagation through the soil profile are being tracked for effects on multiple biogeochemical processes (Pohlmann et al.).

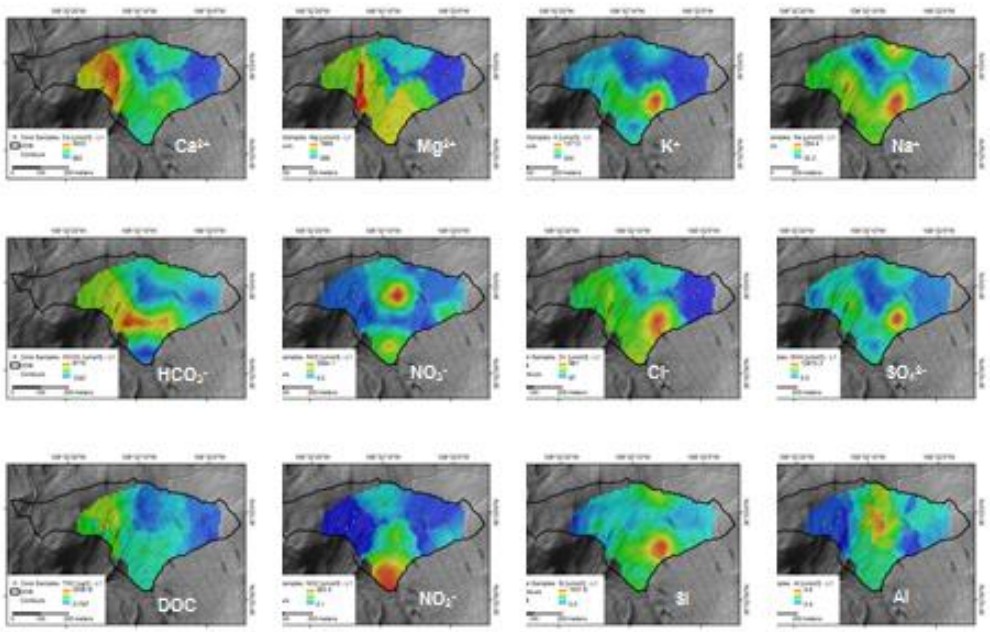

Figure 28. Soluble major ion concentration distributions in the surface 0-2 cm depth of the JRB mixed conifer ZOB following the Thompson Ridge fire (same sample locations as shown in Fig. 10 (Pohlmann et al.).

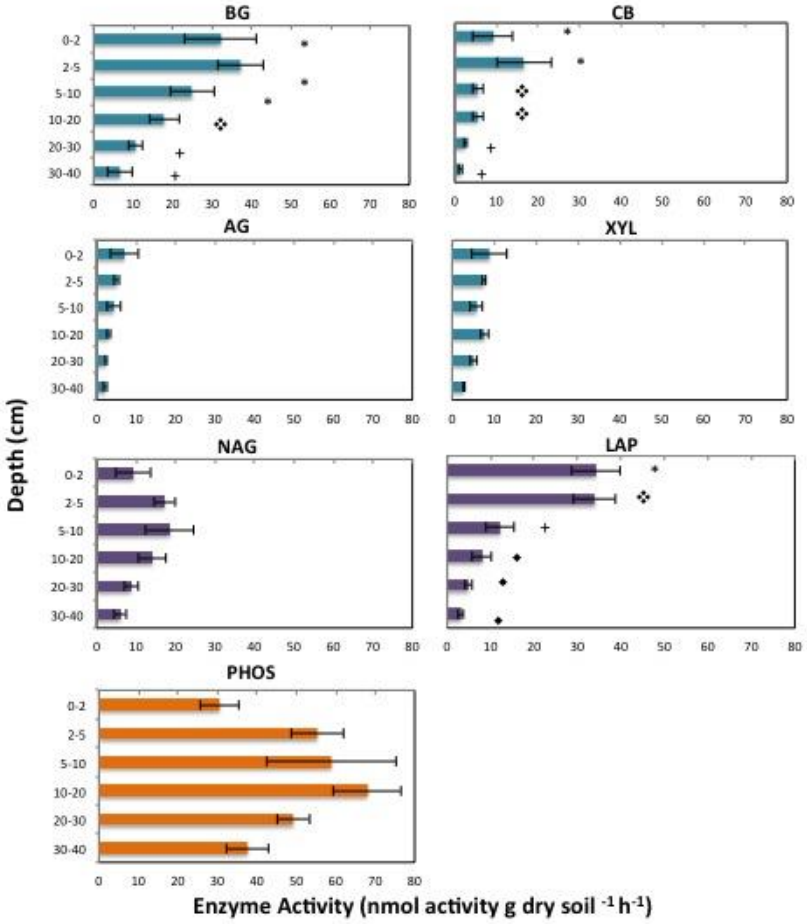

Figure 29. Potential enzyme activity decreases with depth at approximate mean summer soil temperature (15°C) for enzymes β-Glucosidase (BG), β-D-Cellobiohydrolase (CB), and Leucine aminopeptidase (LAP). Here, we see a pattern of decreasing potential activity with increasing soil depth for enzymes BG, CB and LAP that are involved in the degradation of sugar, cellulose and proteins respectively. Their activities are used to gain insight into microbial degradation controls over C and N substrates (Fairbanks et al.)

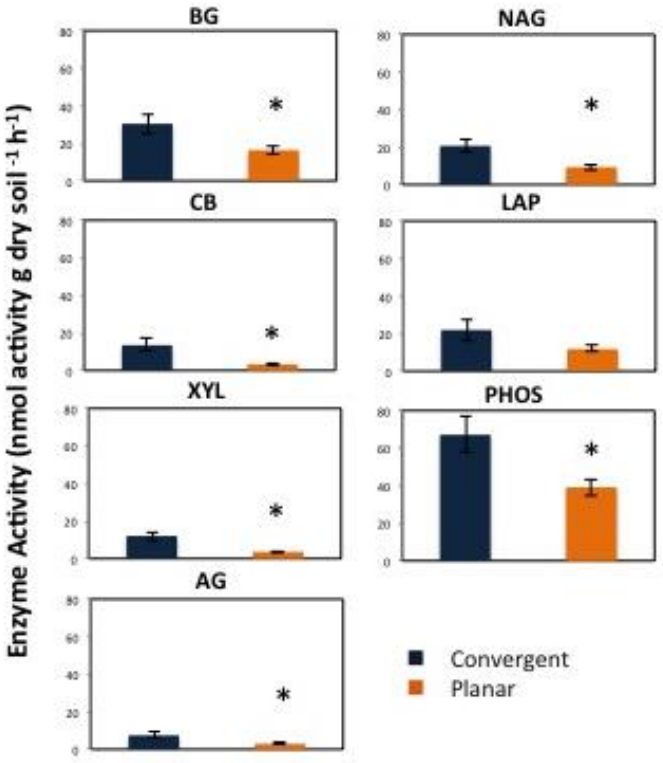

Figure 30. Potential enzyme activity is higher in convergent sites relative to planar sites. Differences in enzyme activity varied with landscape position, specifically convergent versus planar landscape forms. Convergent sites had higher potential enzyme activity for all enzymes assayed with the exception of LAP, for which landscape effect was not statistically significant. These preliminary results indicate that landscape position is likely to have a strong effect on biologically mediated decomposition processes, possibly a result of increased microbial biomass within convergent sites (Fairbanks et al.).

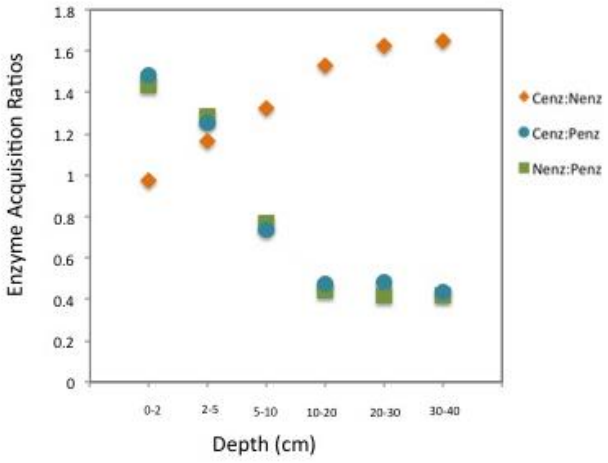

Figure 31. Stoichiometry of potential enzyme activities (derived from data in Fig. 13) shows variance in resource acquisition potential with depth. C_{enz}, N_{enz}, and P_{enz} represent mean potential enzyme activities of (BG+CB+XYL+AG), (NAG+LAP), and PHOS, respectively, at 15°C, the mean summer temperature at the site (Fairbanks et al.).

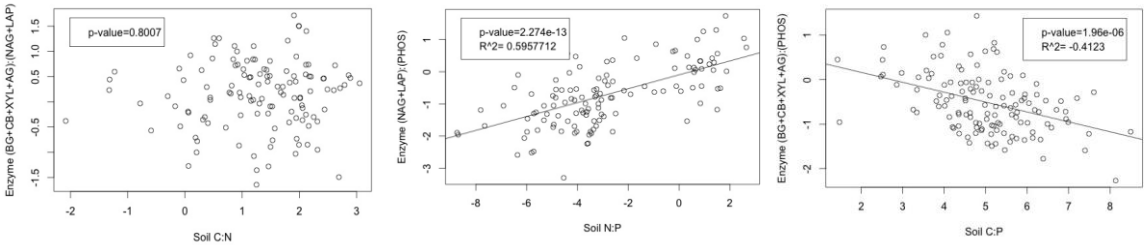

Figure 32. Relationship between soil C:N, C:P, and N:P and corresponding ratio of potential enzyme activity. Enzyme C, N, and P are (BG+CB+AG+XYL), (NAG+LAP), and PHOS respectively assayed at 15°C. Data are log-transformed to improve linear regression fit (Fairbanks et al.).

Table 4. Summary of p-values resulting from ANOVA pairwise comparison model analysis for potential enzyme activities assayed at 15°C. Landscape position (LP) represents convergent vs. planar landscape forms. Results showed no significant interaction between LP and Depth.

Independent Variables	BG	CB	XYL	AG	NAG	LAP	PHOS
Landscape Position (LP)	**0.0118** *	**0.000282** ***	**4.75e-05** ***	**0.000919** ***	**0.0122** *	0.625	**0.0163** *
Depth	**7.68e-07** ***	**0.00022** ***	0.121	0.0672	0.08	**7.46e-11** ***	0.469
LP x Depth	0.83014	0.552	0.4671	0.452256	0.16485	0.270	0.4040

p-values equal to or less than 0.05 are shown in bold
Signif. Codes: 0'***' 0.001 '**' 0.01 '*'

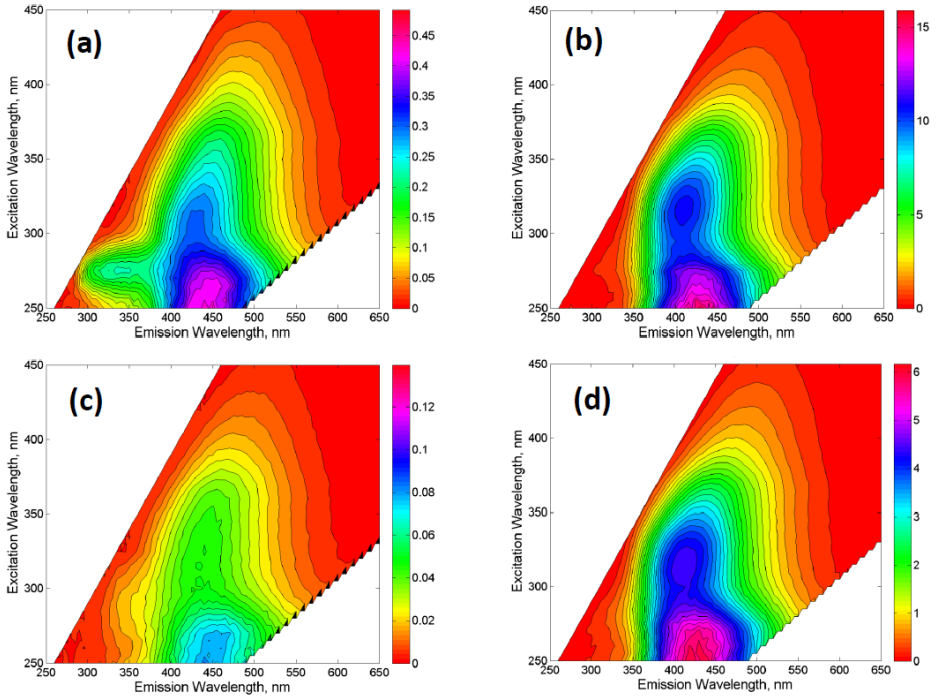

Figure 33. Fluorescence excitation-emission matrices for soil solutions and surface waters in the JRB MC ZOB before and immediately after the Thompson Ridge wildfire of 2013: (a) pre-burn soil solution, (b) post-burn soil solution, (c) pre-burn surface water, and (d) post-burn surface water. The post-burn spectra reflect significantly elevated intensities of soluble aromatic carbon moieties characteristic of benzene polycarboxylic acids (BPCAs).

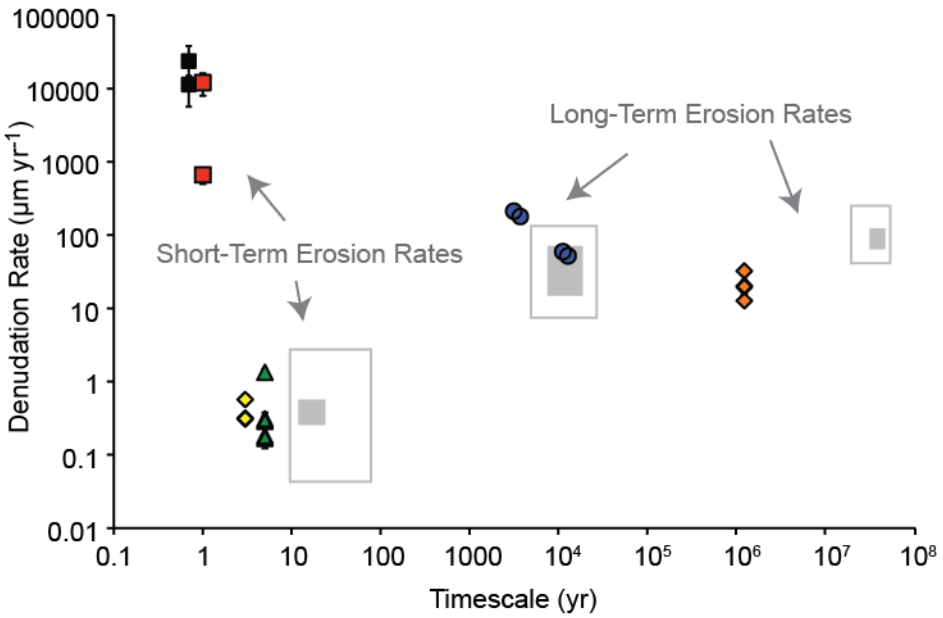

Figure 34. Plot of denudation rates calculated in this study versus timescale. Short-term wildfire-affected, TLS- and ALS-derived DRs (red and black squares), non-wildfire-affected, SSL-derived DRs (green triangles), chemical flux-derived DR (yellow diamonds), and long-term 10Be CRN-derived DRs (blue circles) and DRs derived from incision into a paleosurface (orange diamonds) are shown. Data from Kirchner et al. (2001) also shown in gray squares for comparison (Orem and Pelletier, in press).

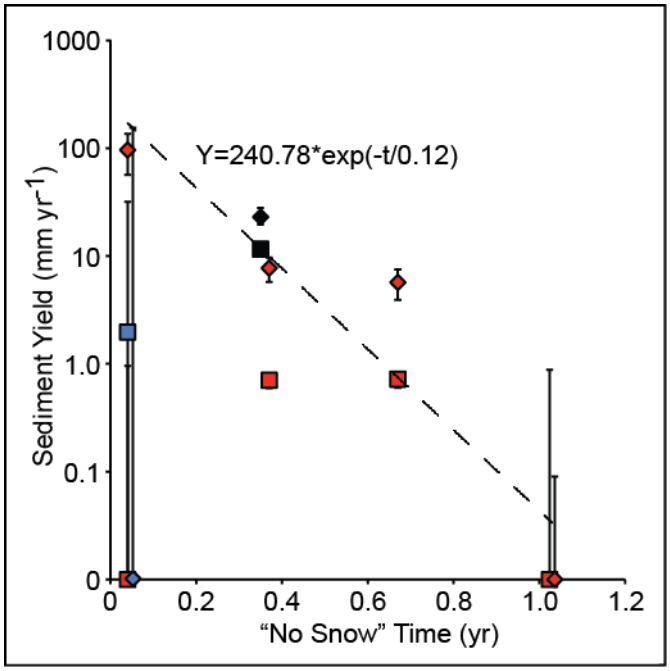

Figure 35. Plot of sediment yields versus "no snow" time for two piedmonts P1 (diamonds) and P2 (squares) surfaces calculated from ALS-to-ALS differencing (black), ALS-to-TLS differencing (blue), and TLS-to-TLS differencing (red). All values derived from net volume changes less than zero set to zero to represent no sediment yield from upland watershed. Error bars shown in black and exponential fit to P1 data from TLS-to-TLS differencing shown in dashed line and equation (Orem and Pelletier).

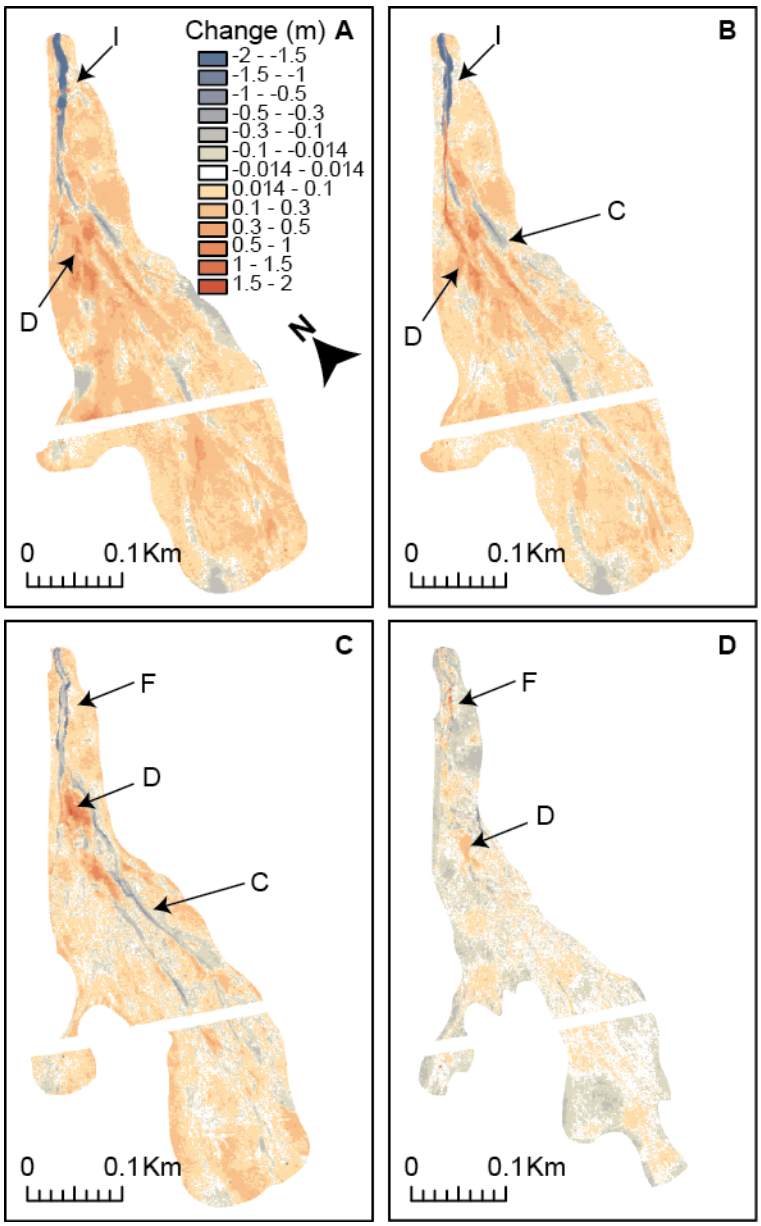

Figure 36. DEMs of difference (DoDs) of a piedmont (P1) through time showing change over the intervals of 8/3/11 to 8/18/11 (A), 8/19/11 to 6/4/12 (B), 6/5/12 to 9/22/12 (C), and 9/23/12 to 5/14/13 (D) from differencing TLS-derived DEMs. Decrease and increase of piedmont surface elevation shown as blue and red, respectively. Important aspects of piedmont surface change are indicated by arrows and labels where I is channel incision, D is deposition, C is channelization (shallow erosion), and F channel infilling (Pelletier et al.).

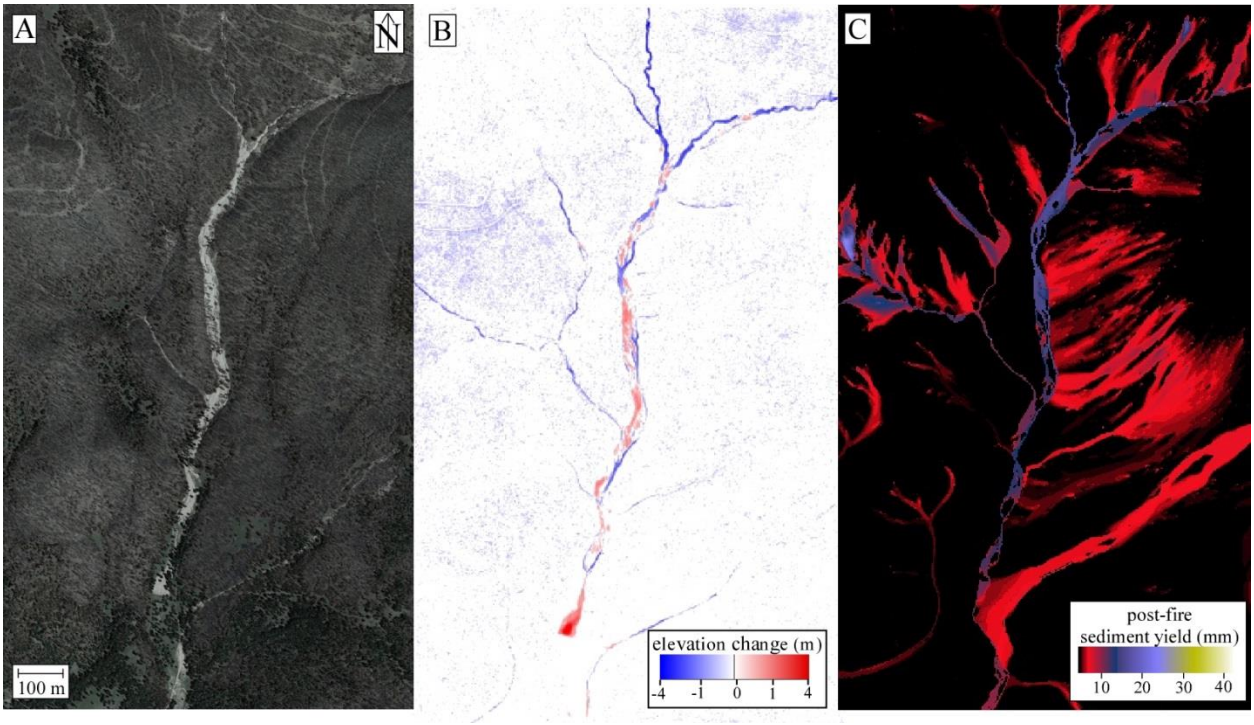

Figure 37. Example of the DEM of Difference (DoD) and associated sediment yield maps for the Valle los Posos study subarea of the Jemez Mtns. (A) Aerial orthophotograph acquired on May 5, 2012. (B) Color map of DoD filtered using magnitude of change, with erosion shown using shades of blue (darker blue represents more erosion) and deposition down using shades of red. (C) Map of sediment yield obtained using the DoD shown in (B) but also filtered by contributing area ($A \geq 0.001$ km^2) (Pelletier et al.).

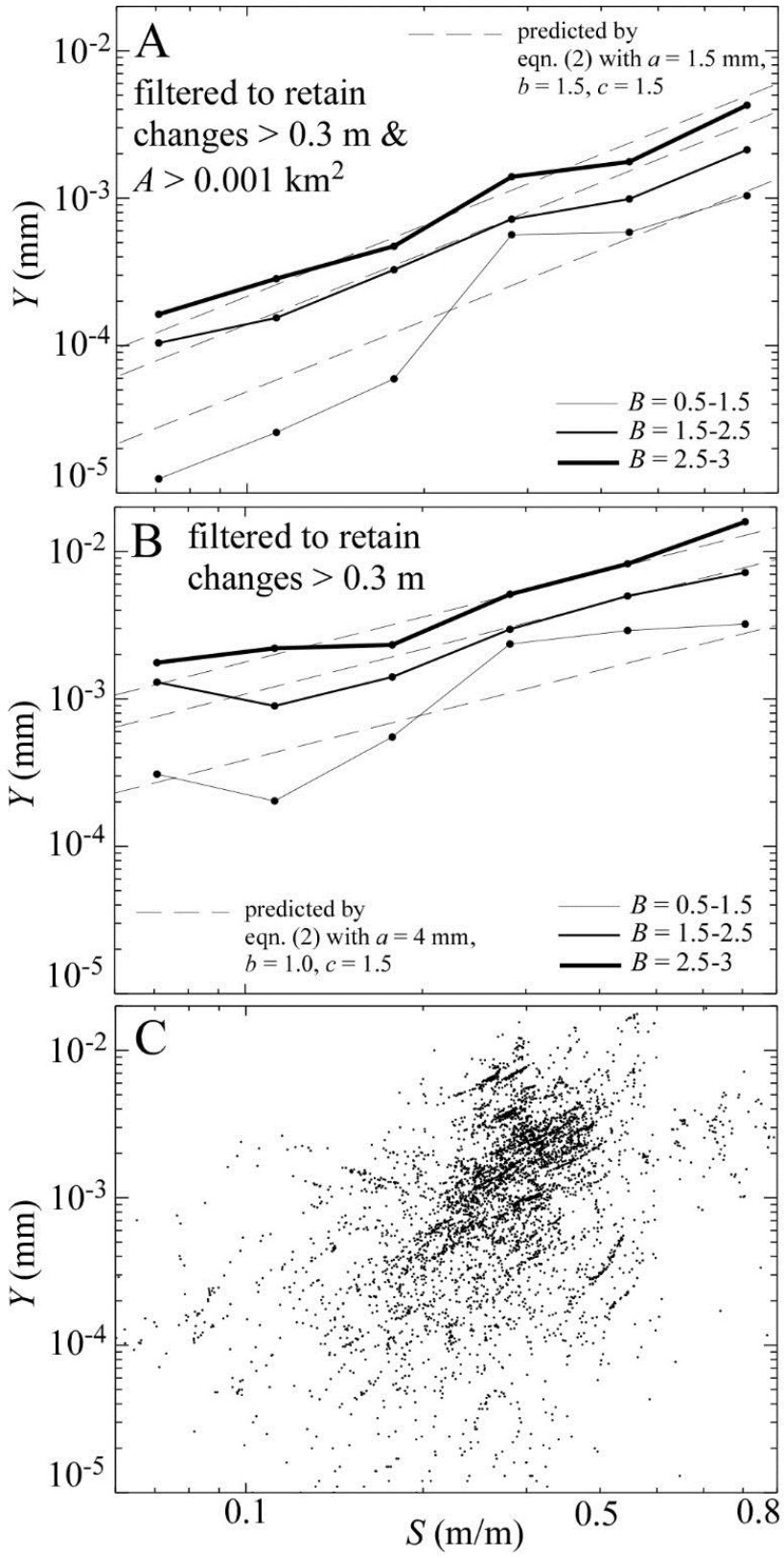

Figure 38. Dependence of average post-wildfire sediment yields, *Y*, on average terrain slope, *S*, and average SBSC, *B,* in drainage basins and comparison of the measurements to the predictions of the empirical model. Bolder line styles indicate data from more severely burned areas. (A) Relationships among measured and predicted average sediment yields, average terrain slope, and average SBSC using the DoD filtered for both magnitude of change and contributing area. Dashed lines show predictions of eqn. (2). Measured data are shown using solid (i.e. un-dashed) lines joining the circles. Note logarithmic scales on both axes. Averaging was performed in six logarithmically spaced bins of slope centered from 0.07 to 0.7 and three bins of average SBSC (*B* = 0.5-1.5, 1.5-2.5 and 2.5-3). (B) Same as (A) except using the DoD filtered for magnitude of change only. (C) Plot of all sediment yields measured in areas of moderate to high average SBSC (*B* = 2.5-3.0), illustrating the large variability about the mean trends illustrated in (A)&(B) (Pelletier et al.).

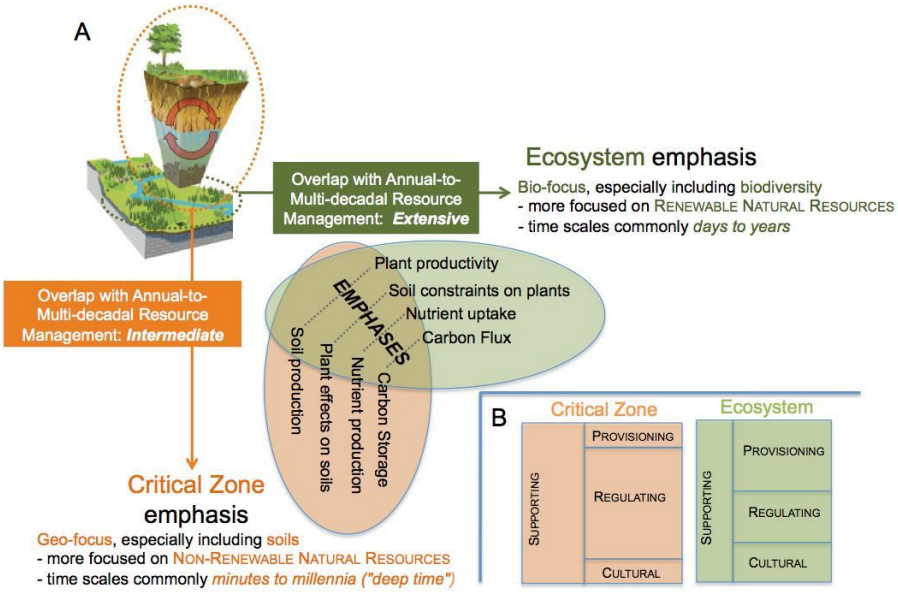

Figure 39. Conceptualization of complementarity between ecosystem and critical zone services. CZ science enables 1) expansion of the scope of ecosystem services by specifying how critical zone processes extend context both spatially and temporally, 2) determination of constraints that limit rates of key processes, and 3) a potentially powerful currency for needed valuation. This figure highlights differences in ecosystem services and critical zone services and the relative focus on different types of services for each (Field et al.).